Republic of IRAQ-BAGHDAD
Ministry of higher Education and Scientific research
University of Technology
Laser and Optoelectronic Engineering Department

Computer Simulations for Ladar Transceiver Performance

A Thesis

Submitted to the Department of Laser and Optoelectronic Engineering
University of Technology in partial fulfillment of the requirements for the degree of Doctor of Philosophy in Optoelectronic Engineering

By

Hamid F. A. Al-Khazraji

Bsc. 1979

Msc. 2002

Supervised by Dr. Hussian J. Abbas

March 2009

بسم الله الرحمن الرحيم

﴿يُدَبِّرُ الأَمْرَ مِنْ السَّمَاءِ إِلَى الأَرْضِ
ثُمَّ يَعْرُجُ إِلَيْهِ فِي يَوْمٍ كَانَ مِقْدَارُهُ
أَلْفَ سَنَةٍ مِمَّا تَعُدُّون﴾

آية 5 سورة السجدة

صدق الله العظيم

♀

Dedicated

To:

My Parents

My Wife

My Sons:

OSAMA

AIAMEN

AMINA

AHMMED

MOHAMMED

SUPERVISORS CERTIFICATION

I certify that this thesis entitled " **Computer Simulations for Ladar Transceiver Performance**" is prepared by Hamid F. Afej under my supervision at the Laser and Optoelectronic Engineering Department, University of Technology in a partial fulfillment of the requirements for the degree of Doctor of Philosophy of Science in Optoelectronics Engineering.

Signature:

Name: Asst. Prof. Dr. Hussain Joma

Date:

CERTIFICATE

This is to certify that this thesis entitled "**Computer Simulations for Ladar Transceiver Performance**" was prepared under my linguistic supervision. Its language was amended to meet the style of the English language.

Signature:

Name: Asst. Prof. Dr. Ahmad Al.Beiruti

Date:

EXAMINATION COMMITTEE CERTIFICATE

We certify that we have read the thesis entitled "**Computer Simulations for Ladar Transceiver Performance**", and as an examination committee examined the student **"**Hamid F. Afej**"** in its content, and that in our opinion it is adequate for the partial fulfillment of the requirement for the degree of doctor of philosophy of Science in Optoelectronics Engineering.

Signature:
Name: Dr. Mohamed R. Mohamed
Title: Professor (Chairman)
Date: / / 2009

Signature:
Name: Dr. Hassan W. Hilou
Title: Assist. Professor (Member)
Date: / / 2009

Signature:
Name: Dr. Jaber S. Aziz
Title: Assist. Professor (Member)
Date: / / 2009

Signature:
Name: Dr. Mohamed Saleh Ahmed
Title: Assist. Professor (Member)
Date: / / 2009

Signature:
Name: Dr. Mohamed Whab Minshid
Title: Assist. Professor (Member)
Date: / / 2009

Signature:
Name: Dr. Hussain Joma Abbas
Title: Assist. Professor (Supervisor)
Date: / / 2009

Approved by Department of Laser and Optoelectronics Engineering, University of Technology.

Signature:
Name: Dr. Mohammed Hussain Ali
Title: Assist. Professor
Head of Laser and Optoelectronics Eng. Dep. University of Technology.
Date: / / 2009

Contents

Acknowledgment

Abstract

List of Abbreviations and Symbols

Chapter 1

General Introduction of Laser Radar

1.1 Introduction…… 1

1.2 Literature Survey …….. 3

1,3 The Aim of the Research……. 6

1.4 Thesis Layout…….. 6

Chapter 2

The Principle of Laser Radar

2.1 Introduction……...… 8

2.2 Laser Radar Principles of Operation...……. 8

2.1 Signal Transmission..……. 10

2.2 Propagation Effects…….. 13

2.3 Target Interaction……. 15

2.4 Signal Reception…… 19

4-1 Coherent Detection…… 20

4-2 Direct Detection……. 24

Chapter 3

Theoretical Background for System design

3.1 Introduction……. 28

3.2 Range Accuracy…… 28

3.3 Radar Range Equation……. 29

3.4 Coherent Detection…….. 35

3.5 Pulse Compression…… 38
3.6 Coherent Integration…….. 41

Chapter 4

Mathematical Model of the System

4.1 Introduction……. 43
4.2 System Block Diagram…….. 43
2-1 The Transmitter…….....…….. 44
1-1 The Waveform Generator...……... 44
1-2 The RF Section of the Transmitter……. 44
1-3 The Optical Section of the Transmitter...…….. 45
2.2 The Receiver.....…….. 46
2 -1 The Optical Section of the Receiver……...… 46
2 -2 The RF Section of the Receiver……..... 46
4.3 Mathematical Modeling of the System…… 48
4.4 Signal Processing……. 54

Chapter 5

Simulation of the System Using Matlab Package and Results

5.1 Introduction…… 56
5.2 Receiver—Simulation and results……... 56
5.3 System Parameters and Block Diagram……. 61
5.4 The Effects of Coherent Integrations on the Output SNR of the System…… 74
5.5 The Effects of Varying Modulation Index on the Minimum Detectable Optical Input Power for the System…… 75
5.6 The Effects of Varying Noise Equivalent Power, NEP, on the Minimum Detectable Optical Input Power for the System… 77

5.7 The Effects of Varying Local Oscillator Power, P_lo, on the Minimum Detectable Optical Input Power for the System….. 79

Chapter 6

Conclusions and Future Recommendations

6.1 Conclusions…… 81

6.2 Future Recommendations…… 82

References…… 83

Acknowledgement

I express my thanks and prays to God who always helps me in all simple and hard moments.

I would like to express my thanks, and deep appreciation to my supervisor, Asst. Prof. Dr. Hussain J. Abbas, for his helpful comments and stimulating discussions throughout the period of this work.

Finally I am very grateful to my family for their patience and encouragement throughout this work. My thanks are due also to all those who helped me throughout the period of this work.

.

Abstract

Laser radar systems play an increasingly important role in global climate change monitoring applications. The fine spatial and range resolution capabilities of laser radar systems make them specially qualified for this work. The current generation of laser radar systems employs short-duration; high peak power pulses, typically using modest pulse repetition frequencies to prolong the limited laser life times associated with such applications. The feasibility of a concept that uses a laser source which produce CW light at 1319nm wavelength and has a maximum power output of 20 dBm and a spectral width of 5kHz modulated by a chirp signal of duration 40μs and band width of 260MHz to achieve a theoretical range accuracy of 10 cm and resolution of 0.576m compatible to short-duration, high-peak power systems have been demonstrated. Through analysis and calculations the results of using optical coherent detection, RF pulse compression and coherent integration shows improvement signal-to-noise ratio (SNR) of 94dB, 40dB and 10dB respectively, these realized receiver sensitivities that makes the system compatible with low peak power laser system. After determining the ladar parameters and completion of mathematical modeling a Matlab simulation program has been used to predict the behavior of ladar under different conditions with different parameters. The results that were predicted from the simulation are the effect of modulation index, noise equivalent power (NEP) and the optimum value of the local oscillator power on the minimum detectable power. It clears from the that the better minimum detectable power of the received signal is obtained by using the higher value of modulation index (which is 1), the system can detect weaker signal when the NEP is small and local power value is to be chosen as high as possible to detect weak signals.

List of Abbreviations and Symboles:

AFCRL	Air Force Cambridge Research Laboratories
AOM	Acousto-Optic Modulator
AMCW	Amplitude-Modulated Continuous-Wave
a	Modulation index of the chirp waveform ($0 < a \leq 1$)
A	Amplitude of the transmitted signal [V]
A_{ap}	Effective receive aperture area ($\pi D2/4$) [m^2]
A_c	Amplitude of the chirp [V]
A_{ill}	Illuminated target area [m^2]
A_{tx}	Amplitude of the transmitted signal [V]
B	Pulse bandwidth [Hz]
B_l	Bandwidth of the first bandpass filter [Hz]
B_{rec}	Receiver bandwidth [Hz]
c	Speed of light [m/s]
CLR	Coherent Laser Radars
CNR	Carrier-to-Noise Ratio
CW	Continuous
DAS	Differential Absorption and Scattering
DC	Direct Current
DOE	Department of Energy
DTED	Digital Terrain Elevation Data
D	Receive aperture diameter [m]
E_{sig}	Electric field incident on the detector [V/m]
E_r	Electric field vector due to the received signal
E_{lo}	Electric field vector due to the local oscillator

EOSL	Electro-Optic Systems Laboratory
FFT	Fast Furrier Transform
f_{car}	Carrier frequency [Hz]
f_s	Frequency shift of the LO signal [Hz]
f_{start}	Starting frequency of the chirp [Hz]
f_{TX}	Optical frequency of the transmit signal [Hz]
GALE	Giant Aperture Lidar Experiment
GLAS	Geosciences Laser Altimeter System
G_a	Optical amplifier gain
G_t	Transmitter antenna gain
HITRAN	High-Resolution Transmission Molecular
IF	Intermediate Frequency
I	Average output current of the photo diode [A]
k	Chirp rate [s^{-2}]
K_a	Aperture illumination constant
ladar	Laser Detection and Ranging
Lidar	Light Detection and Ranging
LITE	Lidar In-space Technology Experiment
Lo	Local
LPF	Low-Pass Flter
MZM	Mach-Zehnder Modulator
m(t)	Chirp waveform [V]
NEP	Noise Equivalent Power
N	Number of signals averaged
n(t)	Noise term [V]
OFA	Optical Fiber Amplifier
OPO	Optical Parametric Oscillator

PRF	Pulse Repetition Frequency
p(t)	Local oscillator signal [V]
P_LO	Local oscillator power
P_{input_opt}	Input optical power
P_{lo}	Local oscillator power [W]
P_n	Noise power in the electrical domain [W]
P_r	Received optical power [W]
P_{sig}	Signal power in the electrical domain [W]
P_t	Transmitter optical power [W]
q	Electron charge [1.6 ×10−19 C]
q(t)	Transmit signal [V]
RF	Radio Frequency
RMS	Root-Mean-Square
$\Re$	Photodiode responsivity [A/W]
R	Range to the target [m]
r(t)	Received signal [V]
SNR	Signal-to-Noise Ratio
s(t)	Detected signal [V]
UV	Ultraviolet
u(t)	Output of the first bandpass filter [V]
v(t)	Output of the linear detector [V]
w(t)	Output of the second bandpass filter [V]
x(t)	Dechirped signal [V]
y(t)	Signal to be signal processed [V]
α	Round-trip loss factor ($0 < \alpha < 1$)

γ	Polarization difference between received signal
η	Detector efficiency ($0<\eta<1$)
η_{sys}	System transmission factor
$\theta_n(t)$	Random phase that follows a uniform distribution
λ	Wavelength [m]
μ	Modulation index
ρ_t	Target reflectivity
ϕ_c	Chirp start phase [radians]
ϕ_{TX}	Phase of the optical transmitted signal [radians]
ϕ_{RX}	Phase of the received signal [radians]
φ	Phase difference between signal and LO [radians]
φ_{LO}	Starting phase of the LO signal [radians]
$\varphi_{optical}$	Phase of the optical signal [radians]
φ_{st}	Starting phase of the waveform [radians]
σ_R	Range accurcy [m]
σ	Effective target cross section [m^2]
τ	Round-trip signal travel time [s]
Ω	Scattering solid angle of target [Sr]
ω_{lo}	Local oscillator frequency [radians/s]

Chapter One

General Introduction of Laser radar

1.1 Introduction:

Lidar, laser radar, optical radar, and ladar are all names used for "radar" systems utilizing electromagnetic radiation at optical frequencies. The radiation used by laser radars is at wavelengths which are 10,000 to 100,000 times shorter than that used by conventional radar [1]. Radiation scattered by the target is collected and processed to yield information about the target and the path to the target. Early conventional and laser radars observed only the intensity of the collected radiation and the time delay from transmission to collection. Modern laser radars also observe intensity and time delay. However some, called "coherent laser radars (CLR)," record information about the phase of the scattered radiation with respect to a local reference [2]. Laser radars may be continuous-wave (CW) or pulsed, focused or collimated. CW laser radars are used when the signal may be integrated over long time periods and when the target is nearby. They are convenient to use when measuring average properties of the path to the target. Focusing is mainly used with CW laser radars to permit them to make a more sensitive measurement over a smaller span of ranges. Pulsed laser radars use much higher power levels during the laser pulse than can be maintained with a CW laser, producing higher signal-to-noise ratios for the collected radiation. Pulsed lidars are usually chosen for long-range remote sensing and when long signal integration is impractical [3] .

Laser radars may also be bistatic or monostatic. Bistatic sensing requires the maintenance of two locations: one for the transmitter and one for the receiver. Monostatic sensing needs only one location to operate. Monostatic sensing is preferred for most scientific measurements because:

- alignment and pointing are more straightforward
- there is only one instrument

- one location to staff
- one location from which to transmit and receive data

The location of a measurement taken by a monostatic, pulsed, laser radar is determined by knowledge of the laser pointing direction, and of the time delay between the firing of the laser pulse and the detection of the signal [4].

The basic measurement made by a ladar device is the distance between the sensor and a target surface, obtained by determining the elapsed time between the emission of a short-duration laser pulse and the arrival of the reflection of that pulse (the return signal) at the sensor's receiver. Multiplying this time interval by the speed of light results in a measurement of the round-trip distance traveled, and dividing that figure by two yields the distance between the sensor and the target. When the vertical distance between a sensor contained in a level-flying aircraft and the Earth's surface is repeatedly measured along a transect, the result is an outline of both the ground surface and any vegetation obscuring it. Even in areas with high vegetation cover, where most measurements will be returned from plant canopies, some measurements will be returned from the underlying ground surface, resulting in a highly accurate map of canopy height [5].

Key differences among ladar sensors are related to the laser's wavelength, power, pulse duration and repetition rate, beam size and divergence angle, the specifics of the scanning mechanism (if any), and the information recorded for each reflected pulse. Lasers for terrestrial applications generally have wavelengths in the range of 900–1064 nanometers, where vegetation reflectance is high. In the visible wavelengths, vegetation absorbance is high and only a small amount of energy would be returned to the sensor. One drawback of working in this range of wavelengths is absorption by clouds, which impedes the use of

these devices during overcast conditions. Bathymetric ladar systems (used to measure elevations under shallow water bodies) make use of wavelengths near 532 nm for better penetration of water. Early ladar sensors were profiling systems, recording observations along a single narrow transect. Later systems operate in a scanning mode, in which the orientation of the laser illumination and receiver field of view is directed from side to side by a rotating mirror, or mirrors, so that as the plane (or other platform) moves forward, the sampled points fall across a wide band or swath, which can be gridded into an image [6].

Two main detection schemes can be identified in laser radar systems; coherent and direct-detection. In coherent detection, the phase information is preserved. The returning signal is mixed with a local oscillator and the signal at the difference frequency is detected. These types of systems are common for aerosol measurements, and velocity and vibration measurements with very high accuracy. In direct-detection systems, the phase information is lost as the returning signal is simply collected on a detector. Direct-detection laser radar systems are less complex and are common in 3D imaging applications. There are several principles for direct-detection 3D imaging laser radar; scanning, staring and gated viewing [7,8].

1.2 Literature Survey:

The introduction of lidar principle dates back to pre-laser times. LIDAR actually started with CW searchlight using geometry to determine altitude. The invention of lasers pushed ladar to a whole new level - modern laser remote sensing. Modern ladars have various formats and utilize different ways to determine altitude and range precisely. Ladar started in the pre-laser times in 1930s with searchlight beams, and then quickly evolved to modern ladars using nano-second laser pulses. . Great

strides were made both in the development of ladar technologies/systems, and in the sophistication of their applications [9]. In 1980 Takashi T. et al analyzed the efficiency in the optical heterodyne detection of an Airy signal field with Gaussian local oscillator field with consideration of the effect of wavefront of both fields [10]. K. F. Hulme et al. in (1981) compared the sensitivities of heterodyne and direct detection systems at co_2 laser wavelengths for a co_2 laser range finder [11]. I. Renhorn et al. in (1983) described the design, calibration and performance of a cw coherent laser radar test bed [12]. J. Salzman and A. Katzir in (1984)applied a new method for calculating the heterodyne efficiency of an optical receiver to specific optical systems looking through a turbulent atmosphere [13]. In the same time J. Bilbro et al. in (1984) used a coherent doppler ladar to measure the 2-dimensional wind field in a number of different atmospheric situations [14]. In (1986) Bilbro et al. presented an important advance in ladar was the recognition that the spectra of the detected radiation contained highly specific information related to the species, which could be used to determine the composition of the object region [15]. Thomas J. Kane et al. in (1987) built a coherent laser radar system operating at the 1.06μm Nd:YAG laser wavelength to detect Signals scattered from clouds at a range of 2.7km and from atmospheric aerosols at a range of 600m [16]. In (1989) Walter L. Tucker et al. studied and evaluated heterodyne efficiencies of optical detector using combinations of planar, airy, and Gaussian signal and local oscillator fields [17]. Rao et al. in (1990) measured the time of flight of laser pulse [18]. In the same time Ullrich and Andreas presented the design and realization of a Doppler radar with a CO2 laser [19]. Pleshano et al. in (1993) investigated the implementation of coherent resption in laser surveillance radar [20]. Fung in (1994) presented the performance of pulsed –imager operation of a coherent laser radar system by evaluating

via computer simulations [21]. Huffaker et al. in (1996) used coherent ladar systems for the remote measurement of atmospheric wind velocity [22]. Der et al. in (1997) described a computer simulation of atmospheric and target effects on the accuracy of range measurement using pulsed laser radar [23]. Ikuta et al. in (1999) studied the improvement of an infrared radiation detection and ranging system [24]. Bryan Blair in(1999) designed and developed at NASA's Goddard Space Flight Center _GSFC[25]. Steinvall in (2000) evaluated laser radar cross sections for a number of ideal target [26]. Avril in (2000) discussed applications irregularly distributed scanning laser altimeter data need to be rasterised - such as for use in GIS systems and for creating DEMs [27]. Andreas Olsson in (2003) presented application of coherent laser radar to find a robust and reliable system for target recognition [28]. Robert et al. (2004) simulate the effect of turbulence on the phases and amplitudes of laser beams will aid the development of a practical synthetic aperture ladar (SAL) [29]. Lars et al. in (2005) predicted laser beam propagation effects in the atmosphere is of importance for laser countermeasures and related applications [30]. Vesna Ducic in (2006) described The performance of the classification algorithm was checked manually on 500 points randomly distributed and on several test zones selected over the study area [31]. Benjamin Koetz et al. in (2006) described The introduction of prior information on the canopy structure derived from large footprint LIDAR observations significantly improved the retrieval performance relative to estimates based solely on spectral information [32]. Wallace et al. in(2006) demonstrated on simulated and real data from amulti-spectral ladar system, and showing that the return

parameters can be estimated to a high degree of accuracy[33]. Qing et al. in (2008) presented a new method for the weak signal detection in the laser radar [34].

1,3 The Aim of the work:

The main aim of this work as follows:

1- Study, analyze and mathematically modeling ladar system that uses less peak power, long pulse duration with using coherent detection, RF pulse compression and coherent integration techniques.
2- Simulate the modeling system using Matlab package program V.7 to predict the behavior of the system design under different conditions or with different parameters.
3- Investigate the results of the simulation for the observation of globale climates.

1.5 Thesis Layout:

This research documents the progress of the project and steps taken to achieve the goal given above. It is divided into six chapters. The first chapter is the general introduction of laser radar and provides objectives to be achieved, literature survey and a brief explanation of the system improvements. The second chapter is an overview of the principle of laser radars. Chapter three deals with the theory section and provide theoretical background for the concepts employed in the project. It also includes step-by-step the analytical explanation of the concepts and formulatic analysis of the signals used in the system. Chapter four deals with detailed description of proposed system. Chapter five presents the simulations that predicted the behavior of the system under different conditions or with different parameters to find the best way to bring the

ladar into reality, and Chapter six presents the conclusions and recommendations for future work.

Chapter Two

The Principle of Laser radar

2.1 Introduction:

A ladar, or laser radar, system operates on the same principle as a radar system, but uses light instead of microwave radiation. Accordingly, it delivers similar remote sensing information, but with different characteristics due to the much shorter wavelengths. Below are sections that include an explanation of principles of operation of laser radar as well as the explanation of the process by which the signal returns are formed into four phases, signal generation occurs at the transmitter, signal propagation, target interaction, and signal reception at the receiver.

2.2 Laser Radar Principles of Operation:

In basic principle all radars are similar. In the idealized case, a transmitter unit emits a directed beam of electromagnetic radiation in a controlled direction [35]. A collection of objects in the path of the beam interacts with the radiation in a manner characteristic of the objects, generating a reflected signal. The reflected signal propagates back to the receiver, which may be co-located with the transmitter, and is detected and processed in the hope of obtaining information about the objects illuminated. The direction of the transmitter beam may then be changed and the process repeated to build up a two-dimensional image of the composite field-of-view, with each measurement corresponding to a pixel of the resulting image [36]. The objects may comprise one or more target objects-objects in which the radar operator is interested-and additional objects, referred to as clutter, which only serve to obscure the picture. Anything other than targets and clutter which results in a received signal is termed background. Note that what constitutes a target and what constitutes background or clutter is somewhat arbitrary and application-dependent-hence the difficulties associated with target recognition and

detection. In general radar's performance is quantified in terms of resolution, accuracy, and precision [37].

One can break down the process by which the signal returns are formed into four phases, as depicted in Figure(2.1). Signal generation occurs at the transmitter and dictates the temporal, spatial, and directional characteristics of the original signal; signal propagation includes the effects of propagation of the signal from the transmitter to the target and from the target to the receiver; target interaction includes the sometimes-complicated effects resulting in generation of a reflected signal, some part of which propagates to the receiver; and signal reception includes the detection and processing of the reflected signal (after propagation to the receiver). up to the point at which received data is recorded. The laser radar and the radar are monostatic-that is, the transmitter and receiver share an antenna (or optics), so that the transmitter and receiver are co-located from the perspective of the target or bistatic, with transmit apertures distinct from (though in close proximity to) the receiver apertures. In the rest of this section we consider laser radar in particular, though much of the discussion applies to conventional radar as well [4].

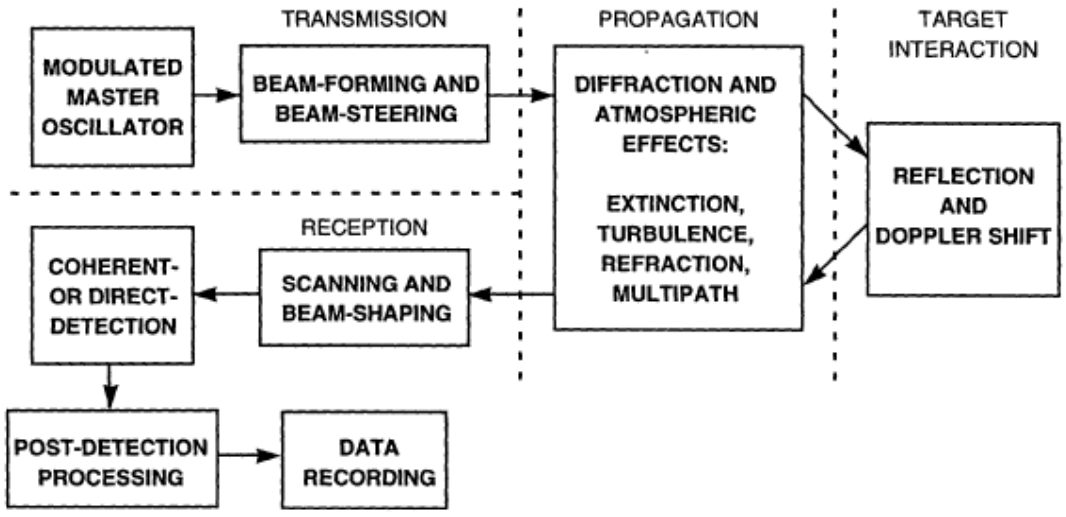

Fig. (2.1): Four stages in the formation of a radar echo [4]

2.2.1 Signal Transmission:

In the signal transmission phase include the events controlling the time and frequency dependencies of the original signal, its initial spatial profile, and its directional characteristics, including any patterns of directional variation with time. The transmitter thus includes a master oscillator acting as a radiation source, along with any modulation, beam-forming, and beam-pointing hardware necessary. The beam-forming optics of the transmitter determines the spot size of the resulting signal beam at the target. For maximum resolution, it is generally desirable to use diffraction-limited optics -that is, optics for which the focusing error resulting from imperfections in the lensing system is smaller than the finite focal spot size required by diffraction from the finite aperture size, given by $2.44\ \lambda\ f/d$, where λ is the transmitter wavelength, f is the focal length of the lens, and d is the lens diameter. The resulting resolution is specified by the beam-spread angle of the transmitter beam in the farfield, as determined by Fraunhofer diffraction. Assuming diffraction-limited optics, the beam-spread full-angle is given by $2.44\ \lambda\ /d$ for a uniformly illuminated circular transmitter aperture of diameter d and transmitter wavelength λ. For monostatic radars, the beam-forming optics are equally important in determining the spatial qualities of the received signal [38].

Scanning optics at the radar transceiver control the directional beam pattern traced out as a function of time. In particular, the forward-looking laser radar achieves two-dimensional imaging of return data by raster-scanning a region of interest in azimuth (parallel to the horizon) and elevation (vertically), while the down-looking laser radar images by scanning in azimuth and allowing aircraft motion to provide the second dimension of variation. When range data are collected and assembled into a 2-dimensional image, the result is 3-D imaging, with the transmitter scanning sweeps providing the two cross-range dimensions and the range

information providing the third dimension. The resulting image can be displayed as a surface plot. A given laser transmitter may be capable of scanning in several different imaging modes, including a wide field-of-view mode for general reconnaissance and a narrow field-ofview mode for obtaining detailed information about a target. Note that, in reality, the scanning process is continuous, not discrete as indicated in the ideal scenario of the introduction. For a bistatic radar, this means that the radar receiver's instantaneous field-of-view is not precisely aligned with the spot illuminated by the corresponding signal beam pulse at the time of arrival of the reflected signal due to scanning motion during time-of-flight. This effect is called "lag angle." For a bistatic radar, if the transmitter and receiver can be independently pointed, it is possible to accommodate the lag angle with appropriate synchronization of the receiver and transmitter scanning systems. In many practical cases, lag angle is only partially compensated for by scanning synchronization, the remainder being accommodated by an enlarged receiver instantaneous field-of-view. Though it must be considered carefully in design of the scanning properties of the radar, by assuming any residual effects of the lag angle to be completely negligible in what follows [4].

The laser-radar master oscillator comprises a laser source and any additional hardware required for temporal modulation of the transmitted signal. The modulation format of the transmit signal is generally chosen to optimize in some sense the amount of information carried by the return regarding the target characteristic being measured; thus different transmit waveforms are used to measure different target characteristics. For example, when detailed relative range information is sought for targets at a well-defined range, an amplitude-modulated continuous-wave transmitter signal (AMCW) can be used. By measuring the phase of the amplitude modulation of the returned signal relative to that of the

transmitter, time-of-flight of the return signal can be determined modulo period *T* of the modulation of the transmitted waveform, and the time-of-flight measurement can be converted to a relative range estimate via

$$R = c.\ T/2$$

Where

c is the propagation speed of the laser signal

T is the measured time-of-flight modulo the waveform period

The ambiguity interval *c.T/2* might be relatively small (say a few meters) for the relative range measurement, but in the absence of noise and for a point target, the precision is limited only by the ability of the receiver to measure phase differences at the frequency of the amplitude modulation. Alternatively, a pulsed waveform can be used for determination of range, with one pulse transmitted per pixel. The rate at which an image can be constructed depends on the pulse repetition frequency (PRF), with higher PRF's allowing faster image formation. However, if the PRF is sufficiently low that the time *T* between pulses is longer than $2\Delta R/c$, where ΔR is the *a priori* range uncertainty, a pulsed transmitter waveform allows absolute ranging-that is, the range ambiguity, given by $cT/2$, is larger than the *a priori* range uncertainty. The minimum distinguishable range difference for a rectangular pulse transmitter waveform is determined by the distance the beam travels along the propagation path (i.e., in the so-called along-range direction) during one pulse width. If each pixel of the target occupies a single range resolution cell, peak-detection can be used at the receiver to estimate the distance to target. If the target is spread over several range resolution cells for each pixel, the pulse returns will be spread over the time interval corresponding to the range extent of the target, and the shape of the received waveform contains information regarding the target and may be important for target

identification-particular cases of this include identification of aerosols or atmospheric pollutants from backscattered returns and recognition of hard targets at ranges at which target features are not spatially resolved. For target velocity measurement, a relatively long-duration, quasi-continuous waveform is required. The frequency difference between the transmitted and returned signals is then measured to determine the Doppler shift imposed by the target on the reflected signal. The resolution of a single measurement is limited by the uncertainty principle to at best the reciprocal duration of the measurement. Thus any particular resolution requirement puts a minimum limit on both the transmitted pulse duration and the dwell time of the radar on each pixel of the target. There is, as a result, a tradeoff between the time required to frame an image and the resolution of the resulting Doppler image [39].

2.2.2 Propagation Effects:

Propagation through the atmosphere from transmitter to target and from target to receiver can be described by three mechanisms [40]: diffraction, extinction, and turbulence-induced effects. Diffraction dictates the minimum beam spread possible in free space for a given aperture size and wavelength; it is thus determined entirely by properties of the transmitter and, for the return path, the target, rather than by any property of the propagation path itself. The aperture size of the transmitter determines the transmitter-to-target diffraction-induced beam spread, whereas the spatial extent and the reflection characteristics of the target determine the target-to- receiver diffraction-induced beam spread. In the absence of turbulence-induced beam spread, the transmitter-to-target diffraction angle determines the angular resolution of the laser radar system. Extinction represents the loss of transmitted beam power both by absorption by atmospheric gases and by scattering by particles

suspended in the atmosphere; extinction causes an exponential decay in the power of the transmitted beam with distance along the propagation path. Extinction rates are strongly dependent on the wavelength of the optical signal; at the near-visible and long-wave IR wavelengths of interest here, fog, haze, precipitation, and high relative humidity can increase extinction significantly above its clear-weather value. In this case the operable mechanisms are absorption by water vapor and carbon dioxide and scattering by water particles [41]. For this reason prevailing weather conditions are noted in the data set indices.

Propagation through cloud cover can also increase extinction rates dramatically. Turbulence-induced effects arise from the presence of random spatio-temporal variations of the refractive index of air due to local temperature variations on the order of 1 K. The relevant effects of propagation through turbulence include transmitter beam spread, target-return beam spread, target-plane scintillation, receiver coherence loss for coherent-detection radars, and angle-of-arrival spread and receiver plane scintillation for direct-detection radars [42, 43].

Transmitter beam spread is largely induced by random phase modulation of the initial spatial phase fronts of the transmitted beam near the transmitter. When the transmitter aperture diameter d exceeds the turbulence coherence length p_0, $d > p_0$, a collimated beam will experience noticeable beam spread due to turbulence. However, for $d << p_0$, diffraction is the primary determinant of beam spread, and turbulence-induced beam spread can be ignored. Target-return beam spread [40] is analogous to transmitter beam spread but occurs for propagation from target to receiver. Target-return beam spread is only non-negligible for those glint returns which would otherwise have very narrow free-space beam spread. Target-plane scintillation manifests itself as a random variation in the illuminating beam intensity in the target plane. It results

essentially from coherent interference of the transmitted beam with itself due to induced spatial phase front modulation. For weak turbulence, the coherence length of the resulting log-amplitude fluctuations is $(\lambda R)^{1/2}$ at range R [39].

As a result of spatial phase-front modulation of the received signal across the receiver aperture, the coherent-detection receiver experiences a reduced mixing efficiency termed receiver coherence loss. Receiver coherence loss is negligible for $d << \rho_0$, but when the receiver aperture size exceeds the turbulence coherence length, the received field's random phase fluctuations across the aperture create a spatial-mode mismatch between the received and local-oscillator fields, and the mixing efficiency can be disastrously affected [42]. For the direct-detection receiver this same turbulence-induced phase-front modulation results in angle-of-arrival spread and receiver-plane scintillation. The angle-of-arrival spread adversely affects received signal power by spreading some of the received signal power outside the receiver field-of-view, but this can be compensated for by widening the field-of-view of the receiver at the cost of increasing the background noise level. Receiver-plane scintillation, which results from self-interference of the turbulence-corrupted received signal phase fronts, can be reduced by increasing the receiver aperture size so that the receiver effectively sums several independent instances of the intensity random variable, thus reducing the effect of scintillation on the receiver output signal [43].

2.2.3 Target Interaction:

It is the interaction between target and incident signal beam which impresses upon the return signal any information it might contain about the target. Unfortunately the interaction between incident signal and target can be quite complicated, and a large body of literature has been

dedicated to its description. For a monostatic radar emitting a quasi-monochromatic, linearly polarized signal beam and observing a hard target at true range *R,* one can describe the reflected beam as the product of a complex target reflection coefficient $T(\bar{p})$ with the incident field in the target plane $\overline{Et}\ (\bar{p}, t)$ [36]:

$$\overline{Er}\ (\bar{p}, t) = T(\bar{p})\ \overline{Et}(\bar{p}, t). \qquad (2\text{-}1)$$

Here $\bar{p}$ is a vector representing the x, y-coordinates in the target plane, $\overline{Er}\ (\bar{p}, t)$ is the complex envelope of reflected field in the target plane, $\overline{Et}\ (\bar{p}, t)$ is the complex envelope of the incident field in the target plane, and $T(\bar{p})$ is the reflection coefficient for the effective plane of interaction represented by the target plane. The shape of the surface of the target is represented by the phase, and the reflectivity by the amplitude, of $T(\bar{p})$. Inherent in this description is the assumption of bi-paraxial propagation, whereby propagation both from transmitter to target and from target back to receiver can be described by paraxial diffraction. There are two limiting cases to be considered for *T* [39]: the pure specular reflection case and the pure diffuse reflection case. Specular reflection is described by a complex target reflection coefficient which varies smoothly in amplitude with $\bar{p}$ and which varies slowly in phase on a scale comparable to the wavelength of the incident signal. Physically, a specular target has a polished surface (smooth on the scale of λ) which may exhibit curvature with a minimum radius larger than the incident beam width. Specular targets give rise to reflections which are strongly directional, and under favorable alignment conditions result in strong return signals at the radar receiver, referred to as glint. Diffuse targets are represented by complex target reflection coefficients with rapidly varying phase. Physically the

surface of a diffuse target is quite rough on the scale of the transmitter wavelength λ, and the resulting reflected field is therefore essentially spatially incoherent. The temporal coherence of the illuminating laser source, however, results in constructive and destructive interference of the field at the receiver, an effect termed speckle. Actual targets generally lie somewhere between the extremes of pure glint and pure speckle targets in the interaction with the incident field.

For a spatially unresolved pure glint target at $\bar{p} = \bar{0}$, take [39]

$$T(\bar{p}) = \lambda \left(\frac{\sigma c}{4\pi}\right)^{1/2} e^{j\theta}\, \delta(\bar{p}) \tag{2-2}$$

Where σ_c is the radar cross section and θ is a random variable representing phase and is uniformly distributed on [0, 2π), θ represents lack of knowledge of the absolute range of the target on a scale of λ. For a pure speckle target [38], $T(\bar{p}) = T_s(\bar{p})$ where $T_\theta(\bar{p})$ is a stationary, zero-mean random function with second moments

$$(T_s(\overline{p1})\, T_s(\overline{p2})) = 0 \tag{2-3}$$

$$(T_S^*(\overline{p1})\, T_s(\overline{p2})) = \lambda^2\left(\frac{p}{\pi}\right)\delta(\overline{p1} - \overline{p2}) \tag{2-4}$$

where p is the target's diffuse reflectivity. The delta function on the righthand side of equation (2-4) implies that the reflected signal is completely nondirectional-that is, the diffuse target reflects equally (on average) in every direction. For the sake of calculation, $T_\theta(\bar{p})$ will be taken to be a circulo-complex Gaussian process. Note that in taking the diffuse reflectivity to be a random function, we are effectively defining the minute surface details of any given target to be noise. To the extent that several different examples of a particular model of tank, for example, would have uncorrelated surface roughness detail on the order of λ, this

is a reasonable choice. As a result, however, even a perfect measurement of $T_o(\bar{p})$, with no additional noise introduced, would be considered a noisy measurement of p. In effect the surface roughness of the real physical target becomes a noise source which obscures the abstract ideal target. Realistic targets are neither pure glint nor pure speckle, but can be represented by a sum of glint and speckle terms.

As a final note about target interaction with the radar beam, remember that the multiplicative model of equation (2-1) is only valid for targets at fixed range from the transmitter. In the case of the Lidar that the transmitter is always in motion, must consider the effect of general relative motion between the transmitter and target. In the inertial frame of the transmitter, one can consider all motion to be due to relative target motion, and on reflection from the target, the signal will also experience a Doppler frequency shift given by [35]

$$v_D = -2\bar{v}\ \hat{\imath}/\lambda \tag{2-5}$$

where v_D is the Doppler frequency shift, in Hertz, experienced by the reflected signal, $\bar{v}$ is the relative velocity of the target in the inertial frame of the transmitter, i is a unit vector pointing along the line-of-sight from transmitter to target, and λ is the wavelength of the laser radar signal. Note the Doppler frequency shift is positive for an object moving toward the transmitter-that is, the received frequency is higher than the transmitted frequency. The Doppler shift is the interaction process that makes possible remote velocity estimation, and the Doppler shift due to the aircraft's motion over slow-moving surface targets must be considered in the design of the receiver if coherent detection is employed [35].

2.2.4 Signal Reception:

The receiver used in the laser-radar system plays a critical role in determining the sensitivity and capabilities of the system. For optical radars, there is a choice of whether to employ direct detection techniques (in which the received signal is detected with a square-law device which responds to incident intensity) or coherent detection techniques (in which the received field is beat against a local oscillator field of nearly the same frequency, and the output signal is proportional to the received field strength) [45]. Coherent detection utilizes the proportionality of the beat term to the local oscillator field strength to provide essentially noiseless pre-detection gain in the ideal case, so that thermal and dark current noises inherent to the photodetector and pre-amplifier are dwarfed by the quantum noise inherent in the signal itself. Thus coherent detection techniques provide superior sensitivity to direct detection under ideal conditions when signal strength is limited. In addition, detection of Doppler frequency shifts associated with interesting target velocities requires coherent techniques. Unfortunately, coherent detection, while directly comparable to the techniques used for decades in radio receivers, is much more difficult to implement than direct detection at optical frequencies. Coherent detection places strict requirements on the spectral purity of the source (i.e., temporal coherence between the LO and the received signal are required) and requires that the received signal and the local oscillator have spatial phase fronts which are nearly perfectly aligned over the active area of the detector (i.e., spatial modes of the LO and received signal fields must be matched). Direct detection therefore has advantages over coherent detection when either source temporal coherence or the spatial phase characteristics of the received signal cannot be strictly controlled, or when complexity or cost are important design issues [44].

2.2.4-1 Coherent Detection:

Coherent detection is employed in the laser radar system; in particular, an optical heterodyne receiver is used, as depicted in Figure (2-2). The optical receiver comprises a local oscillator laser, offset in frequency from the master oscillator by difference frequency v_{ofset}; mixing optics; and a photodetector array. A block diagram of the optical receiver and post-detection processor appears in Figure (2-3). The mixing optics combine the received target return signal with the local oscillator on the active surface of the photodetector array. For optimal detection, the spatial mode of the local oscillator should be perfectly matched to that of the received signal; the degree to which this is achieved is reflected in the heterodyne mixing efficiency. The output of the photodetectors includes a signal at the beat frequency $v_{IF} = v_{\text{ofset}} + v_{Doppler}$ where $v_{Doppler}$ is the Doppler shift associated with the forward motion of the aircraft relative to stationary surface targets. For a pulse-imager transmitting a rectangular pulse of duration t_p, the complex envelope of the IF photodetector output signal, in a convenient normalization, is given by [46]

$$r(t) = y(t) + n(t)$$

where n(t) is a zero-mean circulo-complex white Gaussian noise process of spectral density hv_o/η, representing the local-oscillator shot noise; and y(t) is the received signal component, given by [39]

$$y(t) = \begin{cases} \sqrt{PT} \int d\bar{p}\, T(\bar{p}) \xi_t^2(\bar{p}), & \frac{2R}{c} < t < tp + \frac{2R}{c}; \\ 0 & otherwise \end{cases}$$

where P_T is the peak transmitted power, $\xi_t(\bar{p})$ is the normalized complex field pattern of the transmitted beam in the target plane, and $2R/c$ is the

propagation delay, by assuming that the transmitted field pattern in the target plane is identical to the normalized local oscillator complex field pattern backpropagated to the target plane. It can be shown that the resulting carrier-to-noise ratio (that is, the ratio of average target-return power after IF filtering to average shot-noise power after IF filtering) is given by [46]

$$CNR = \frac{\eta P_T}{h\nu_0 B} \frac{G_T}{4\pi R^2} \frac{\sigma_c A_R}{4\pi R^2} \epsilon\, e^{-2\alpha R} \tag{2-6}$$

for a pure glint target and by

$$CNR = \frac{\eta P_T}{h\nu_0 B} \frac{\rho A_R}{\pi R^2} \epsilon\, e^{-2\alpha R} \tag{2-7}$$

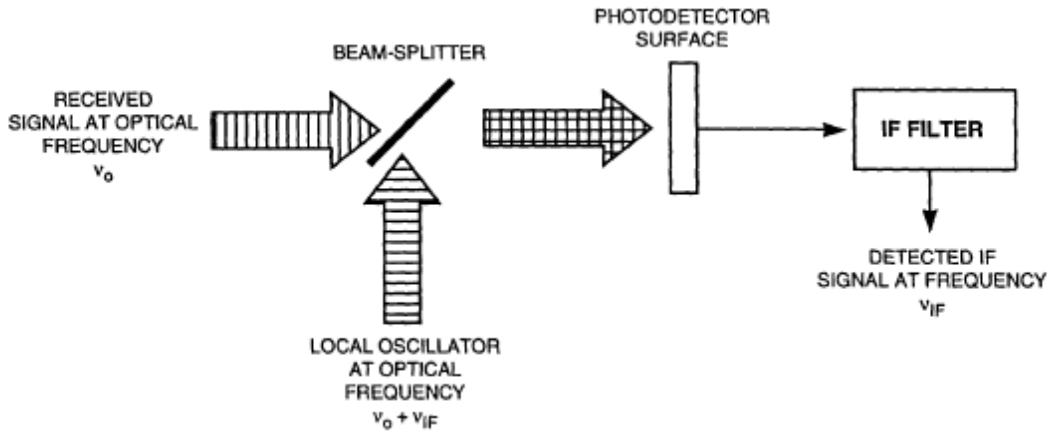

Fig. (2.2): Coherent optical heterodyne detection [46]

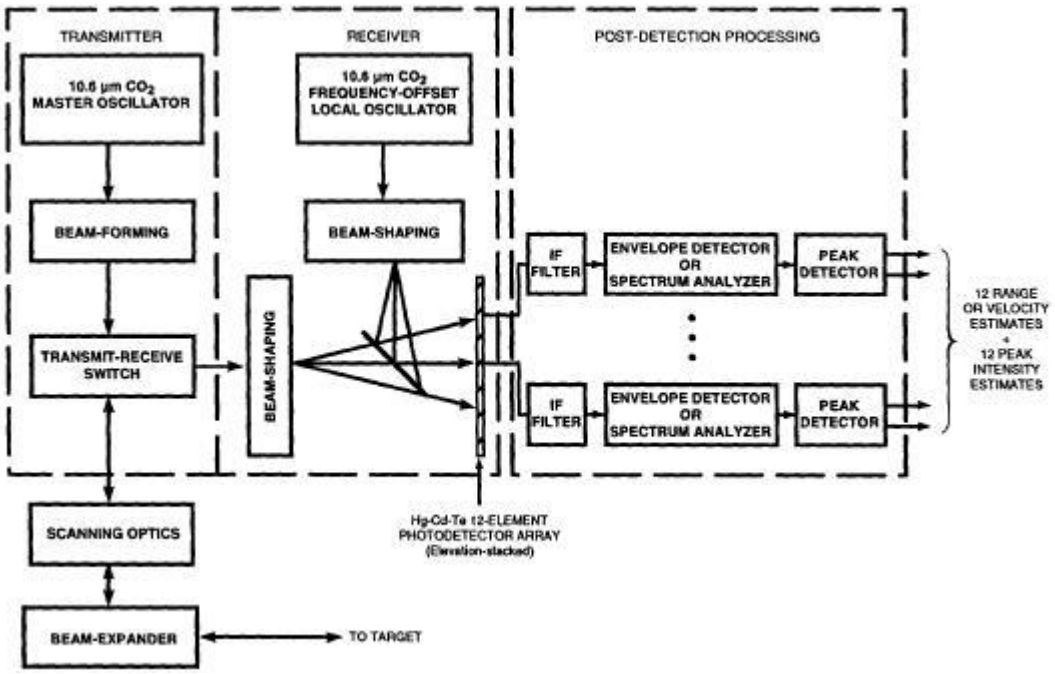

Fig. (2.3): Coherent laser radar receiver block diagram [46]

for a pure speckle target, where P_T represents the peak transmitted power, v, is the center frequency of the transmitted radar signal, B is the bandwidth of the IF filtering stage ($B = 1/t_p$ in this example), G_T is the transmitter antenna gain, σ_c is the radar cross-section for the glint target, A_R is the area of the receiver aperture, ϵ represents the combined heterodyne-mixing and optics efficiencies, α is the atmospheric extinction coefficient, and ρ is the diffuse reflectivity for the speckle target. Ideally the IF output signal from the photodetector is matched-filtered and envelopedetected; the resulting signal at the output of a square-law envelope detector is given by [39]

$$\left|\int_{2R/c}^{t_p+2R/c} r(t)\, d(t)\right|^2 \equiv \lfloor r \rfloor^2$$

If the envelope detector's output is sampled at the exact time corresponding to the propagation delay associated with the target's true

range. An intensity image constructed from these values would then show a signal-to-noise ratio given by [39]

$$SNR = \frac{[\langle |r|2 \rangle - h\nu_0/\eta t_p]2}{var(|r|2)} \qquad (2\text{-}8)$$

where the term subtracted in the numerator represents a constant component of ($1rl^2$) which does not originate from the signal component. The resulting SNR differs in construction from the CNR in that it takes into consideration both the action of the envelope detector and the fact that the signal component **y** of **r** may contribute to the noise by means of the randomness of the target reflectivity T. However, it is the image SNR which is of concern to a viewer of the final image. The intensity-image SNR can be shown to be given by [39]

$$\text{SNR} = \frac{\text{CNR}/2}{1+(CNR)^{-1}+CNR/2SNR_{sat}} \ , \qquad (2\text{-}9)$$

where SNR_{sat} is the saturation value of image SNR and is given by

$$SNR_{sat} \longrightarrow \infty \qquad (2\text{-}10)$$

for a pure glint target and by

$$SNR_{sat} = 1 \qquad (2\text{-}11)$$

for the speckle target case. Thus in the glint target case, the image SNR goes to one-half the CNR value for large CNR, and in the speckle case the image SNR saturates at unity. The CNR differs from the signal-to-noise ratio in that it ignores target-dependent noise in the reflected image due to the noisy nature of the reflection process. In contrast, the image SNR also includes noise introduced by variations in the reflection process which we have chosen to model as random, as mentioned in the target

interaction section. Thus while the CNR relates the technical quality of the receiver output, it tells us little about the quality of the final image; this is the value of the image SNR.

Following the coherent pulse-tone optical receiver is any post-processing electronics which might be required. In the case of range and intensity measurement for hard targets, the filtered IF output is envelope-detected, and a peak detector is commonly used to select the maximum value of the optical receiver's filtered IF output that occurs within a preset range-uncertainty interval. The magnitude of this peak signal value is then digitized and recorded as the intensity value for the given pixel, and the range corresponding to that peak value is digitized and recorded as the range value for that pixel. The process is then repeated for the next pixel. In the case of target velocity measurement, the pre-processing must separate out the different frequency components of the optical receiver's output in order to obtain an estimate of the Doppler shift associated with the target. There are several possible techniques for performing this sorting by frequency, including a discrete filter bank and calculation of the signal's Fourier transform. Some form of peak detection may then be performed on the frequency-sorted return signal to obtain a peak intensity value and velocity value for the pixel. These values are then digitized and recorded, and the process repeated for the next pixel [47].

2.2.4-2 Direct Detection:

Direct detection is employed for some cases in laser radars. In this case the optical receiver comprises an optical interference-type filter to reduce the background radiation incident on the detector followed by photodiode semiconductor detectors. A block diagram of the optical receiver and the post-detection processor used on the laser radars is depicted in Figure (2-4). The most critical component of the direct

detection receiver is the photodetector. The active sensor in the laser radar use semiconductor devices as photodetectors. We provide here a very cursory description of the operation of semiconductor photodiodes. The photodiode detectors we are concerned with have an intrinsic active region sandwiched between p-doped and n-doped regions, and hence are referred to as *p-i-n* detectors. The detector is operated in a reverse-biased mode so as to deplete the intrinsic region of carriers. Photons incident on the detector's active region are then absorbed with probability η, where η is the detector's quantum efficiency. The absorption of a photon moves an electron from the valence to the conduction band of the photodiode, creating a hole-electron carrier pair in the depleted region. The reverse-biased field in the depleted region then causes the hole to drift toward the n-region and the electron toward the p-region of the photodiode [48].

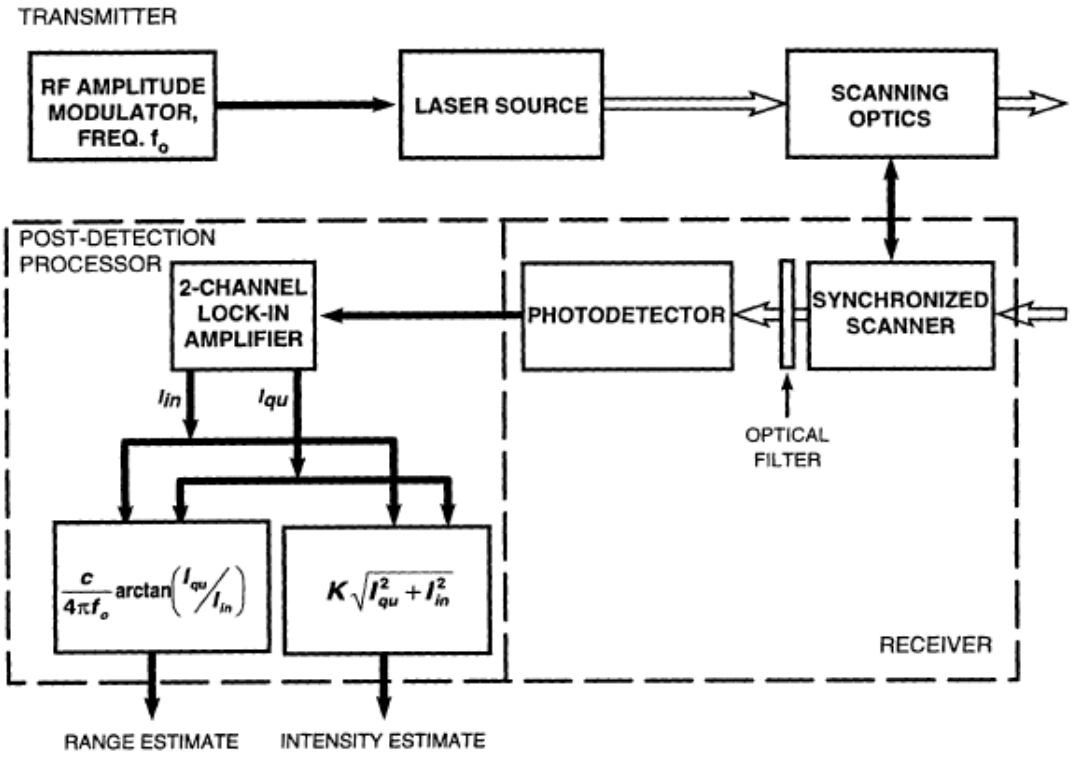

Fig.(2-4) Direct-detection laser radar receiver block diagram [48]

This carrier drift, which ultimately results in recombination of each element of the carrier pair at the edges of the depleted region, results in a spike of photocurrent through the photodiode which is of duration limited

by the carrier transit time across the depletion region. The total amount of charge carried by the current spike is q, the electrostatic charge of the electron, in the case of a standard *p-i-n* photodiode. Note that a macroscopic average current associated with illumination of the detector by a constant optical intensity therefore has associated with it a noise level due to the discrete nature of the carrier creation process. This noise is called shot noise and is quantified by its (single-sided) spectral density, which can be multiplied by the bandwidth of the system to obtain the variance of the noise current [49]:

$$S_{ii} = 2q\bar{I} \tag{2-12}$$

$$\overline{\Delta\, i_{shot}^2} = 2q\bar{I}B \tag{2-13}$$

where q is the charge of a single carrier, $\bar{I}$ is the mean photocurrent, i_{shot} is the shot noise current, and B is the bandwidth of the receiver. We have assumed in Equation [2-12] that the transit time of the carriers is sufficiently short relative to the impulse response of the receiver electronics that the current pulses can be modeled as impulses.

The times at which the discrete charge pulses occur constitute a Poisson process for constant illumination intensity. In the limiting case of an ideal, noiseless detector, shot noise determines the limiting performance of the detector. Its fundamental nature is made apparent by noting that it is ultimately a manifestation of the quantum nature of light.
In the case of an avalanche photodiode (APD), the reverse-biasing electric field is maintained at a sufficiently high strength that the original carriers are multiplied by impact ionization with the lattice, and each of the secondaries so produced is similarly multiplied, until all the resulting carriers drift outside the high-field depleted region. As a result, for the APD, the total charge carried by the current spike associated with any particular photon absorption event is multiplied by a random factor as

compared with the standard *p-i-n* photodiode. This multiplication constitutes the internal gain of the APD [49].

In a real photodiode, there are other sources of noise to be considered as well. The Gaussian thermal noise associated with the load resistor and amplification electronics is one of the more important sources. For many detectors, the shot noise associated with the dark current of the detector (i.e., the current which flows through the photodiode even in the absence of illumination) must be considered. In addition, background radiation, including stray light originating both in the field of view and from the receiver enclosure itself, can be a significant source of shot noise, particularly for detection of thermal radiation, where controlling stray radiation becomes difficult. Finally, for APDs, the random nature of the multiplication process introduces more noise into the detection process and must be accounted for as well. The strength of each of these noise sources is quantified by its spectral density, which is well-modeled as frequency-independent for both thermal and shot noise-that is, the noises are white, and each can be quantified by a single number, the spectral density. The excess noise due to randomness of the photodetector gain is represented by a factor $F \geq 1$ which multiplies the spectral density of the shot noise. In the case of direct-detection AMCW optical receivers, post-detection processing begins with narrowband filtering and separation into in-phase and quadrature components using a lock-in amplifier synchronized to the transmitter's amplitude modulation signal. The two components are further processed to obtain relative range and intensity estimates, which are then sampled and recorded [50].

Chapter Three

Theoretical Background for System design

3.1 Introduction:

Laser radars employ techniques developed for conventional radars at very short wavelengths. The use of shorter wavelengths enables the laser radars to achieve more precise resolution and higher accuracy than microwave radars. To be able to observe the changes in global climate and to measure vegetation characteristics, and aerosol characteristics needed for this project, while still providing the necessary range accuracy, will employ pulse compression, coherent integration and coherent detection techniques. Below are sections that include an explanation of the abbreviations used in the formulas, as well as the explanation of the techniques employed for improving the system performance.

3.2 Range Accuracy:

The laser radar will be designed to achieve the proposed improvements of size and power consumption and sensor flexibility. During the design of the laser radar system, the key parameter is range accuracy. Range accuracy is the expected error in the true range to the target. In general, the required range accuracy is determined by the application. For observing the changes in global climate and to measure vegetation characteristics, and aerosol characteristics, the glaciological community requires 10 cm [51]. The range accuracy is affected by two parameters: effective bandwidth and signal-to-noise ratio (SNR). This is evident from the following representation for range accuracy: [1, 52]

$$\sigma_R = \frac{c}{2B\sqrt{2SNR}} \tag{3-1}$$

where

σ_R = RMS (root-mean-square) error in range measurement [m]

SNR = signal-to-noise ratio at the output of the system

c = speed of light [m/s]

B = pulse bandwidth [Hz]

As can be seen from this equation, increasing the effective bandwidth or improving the signal-to-noise ratio reduces the error in range measurement, thus improving the range accuracy of the system. The bandwidth of proposed system is set at the same value as the one used for the Geoscience Laser Altimeter System (GLAS) system which it's value is 260MHz [51]. It can be increased further to obtain better range accuracy, but this increase might bring some unwanted extra costs to the system. When the bandwidth of the system is increased, this might also increase the processing time of the collected data on board or require more bandwidth to send it to the Earth control point. Because of this extra cost, a reasonable value is chosen for the bandwidth to keep the bandwidth cost low. (A reasonable level is also needed since equation (3-1) is valid for SNRs higher than 10). However, the SNR of the system can be improved by employing methods like pulse compression, coherent integration and coherent detection techniques. To predict the SNR at the photo diode output, therefore ,using radar range equation.

3.3 Radar Range Equation:

From the radar range equation, one can determine the received power and the SNR for a given system configuration. The equation presented has its basis from the microwave radar range equation since principles of electromagnetic propagation are still applicable [1].

$$p_r = \frac{p_t G_t}{4\pi R^2} \frac{\sigma G_a}{4\pi R^2} A_{ap} \eta_{sys} \qquad (3\text{-}2)$$

Where

P_r = received optical power [W]

P_t = transmitter optical power [W]

G_t = transmitter antenna gain

σ = effective target cross section [m^2]

R = range to the target [m]

D = receive aperture diameter [m]

G_a = optical amplifier gain

η_{sys} = system transmission factor

A_{ap} = effective receive aperture area ($\pi D^2/ 4$) [m^2]

The transmitter antenna gain is found using the equation

$$G_t = 4\pi / \theta_T^2 \qquad (3\text{-}3)$$

where

θ_T is the solid angle of the transmitter beam width in steradians [sr].

Since the equation for Gt is only valid for far-field applications, the equation needs to be modified for applications in the near field. Our measurement project is one that operates in the near field, so the necessary adjustments need to be made to obtain a correct model from the radar range equation. The near field is defined as follows:

Range to the target, $R < 2D^2 / \lambda$

where

λ = the wavelength [m]

With the wavelength used in this design, the system operates in the near field. The beamwidth should be modified as follows for the near-field applications[1]:

$$\theta_T^2 = [(\frac{K_a D}{R})^2] + (\frac{K_a \lambda}{D})^2] \qquad (3\text{-}4)$$

where

K_a = aperture illumination constant (a constant used to illustrate the difference between radar and various optical beam width definitions)

The effective target cross section depends on the target reflectivity and illuminated target area. Its representation is as follows: [54]

$$\sigma = \frac{4\pi}{\Omega} p_t \mathrm{A}_{ill} \tag{3-5}$$

where

Ω = scattering solid angle of target [sr]

ρ_t = target reflectivity

A_{ill} = illuminated target area [m^2]

This formula shows that as the target reflectivity gets bigger, the effective cross section increases, which also increases the received power,. For natural extended area targets, one can assume Lambertian scattering, where the scattering occurs uniformly in all directions[55]. The equation for the effective target cross section is reduced to the form below for Lambertian targets, since the value for Ω is replaced with the value for the standard scattering diffuse target having a solid angle of π steradians: [1]

$$\sigma = 4\rho_t A_{ill} \tag{3-6}$$

since the target for this system is intercept the entire beam from the transmitter. This kind of target is called an extended target and it has an illuminated area, A_{ill} , with a range-square dependency, shown below [56]:

$$A_{ill} = \frac{\pi R^2 \theta_T^2}{4} \tag{3-7}$$

while calculating the received power to the system, we should also take the limitations of the equipment into account. This is entered into the radar range equation with the η_{sys} parameter. The optical signal is incident of the photo diode to be converted to an electrical signal. The output current obtained from a photo diode with incoherent (direct) detection may be expressed as [56]:

$$i_{sig} = \Re E_{sig}{}^2 = \Re P_r \tag{3-8}$$

where

$\Re$ = detector responsivity [A/W]

E_{sig} = electric field incident on the detector [V/m]

Responsivity is a measure of the sensitivity of the photo diode and is the ratio of the current output of the diode, Iout, to the incident optical power, Pin, given in the following formula [56]:

$$\Re = I_{out} / P_{in} \tag{3-9}$$

To obtain an expression for SNR one need to obtain the signal power in the electrical domain. The following expression transforms the optical domain signal power, Pr, into the electrical domain signal power, Psig.

$$P_{sig} = \Re^2 P_r{}^2 \tag{3-10}$$

when the signal power in electrical domain is obtained, the expression for SNR at the output of the photo diode can be obtained:

$$SNR = P_{sig} / P_n \tag{3-11}$$

where

P_{sig} = signal power in the electrical domain [W]

P_n = noise power in the electrical domain [W]

As seen from equation(3-10), the value for this received signal power in the optical domain, P_r, affects signal power in the electrical domain, which in turn affects SNR and range accuracy. This SNR is the ratio of the signal power P_{sig} and the noise power P_n measured at the output of the photo diode (at point A), as shown in Figure (3-1).

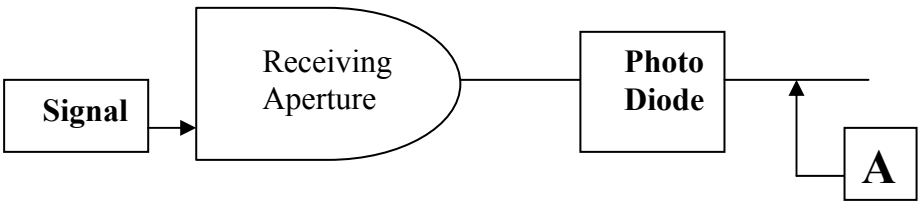

Fig. (3-1): Design showing the point where SNR is measured.

The noise is assumed to come from the photo diode. It is assumed that the noise power, P_n, is due to thermal and shot noise produced in the photo diode. The thermal noise is modeled using the following formula [57]:

$$P_{n-th} = \Re^2 NEP^2 B_{rec} \tag{3-12}$$

where

NEP = noise equivalent power [W/ Hz]

B_{rec} = receiver bandwidth [Hz]

Noise equivalent power, NEP, is given as a performance parameter for photo diodes and is defined as the optical power incident on the diode that will make the SNR equal to 1 for a fixed thermal noise level.

Shot noise is associated with quantization of light energy into photons. The value for shot noise power, $P_{n\text{-}sh}$, can be obtained using the following formula:

$$P_{n-sh} = 2qIB_{rec} \tag{3-13}$$

where

q = electron charge [1.6 ×10−19 C]

I = average output current of the photo diode [A]

The output current has two main components, which are $I_{incident}$ and I_{dark}. The incident current is caused by the incoming photons hitting the photo diode, while the dark current is the output of the photo diode with no input illumination. One can now combine representations for noise power and signal power, to obtain a complete formula for SNR with incoherent detection [57]: $SNR_{incoh} = \frac{\Re^2 P_r^{\,2}}{\Re^2 NEP^2 B_{rec} + 2qIB_{rec}}$ (3-14)

Next one can look at numerical example to obtain a numerical value for the SNR with the parameters chosen to represent the system that will be built. The system parameter values for a lambertian target are as follows [53].

System Parameters

P_t = 10 mW

λ = 1319 nm

D = 1 m

R = 600 km

B_{rec} = 800 MHz

η_{sys} = 0.3

ρ_t = 0.5

$\Re$ = 0.7 A/W

NEP = 2.4×10−11 W/ Hz

G_a = 23 dB

G_t = 7.323×1012

A_{ill} = 0.4852

P_r = 0.165 pW

$I_{incident}$ = 1 μA

I_{dark} = 1 nA

The value for signal power, P_{sig}, turns out to be 1.33 ×10−26 W. The value for the thermal noise power, $P_{n\text{-}th}$, is 2.26×10−13 W. The value for the shot noise power, $P_{n\text{-}sh}$, is 2.56×10−16 W. Since the shot noise term is small compared to the thermal noise, the noise power is assumed to be caused only by thermal noise ($Pn = P_{n\text{-}th}$). These values for signal and noise power give an SNR = 5.88×10−14 , which is about -132 dB. This value of SNR is too low to give the needed range accuracy. Since this is the case, methods for improving the receiver sensitivity will be explored. These methods include coherent detection, pulse compression and coherent integration, which will be employed to increase the sensitivity of the system.

3.4 Coherent Detection:

The coherent detection scheme is similar to the incoherent technique with one exception; in this scheme an optical local oscillator [Lo] signal is coupled to the photo diode during the detection process. When the incoming optical signal reaches the receiver, it is mixed with this local oscillator signal and then passed to the photo diode. A simple diagram for a coherent system is shown below in Figure (3-2).

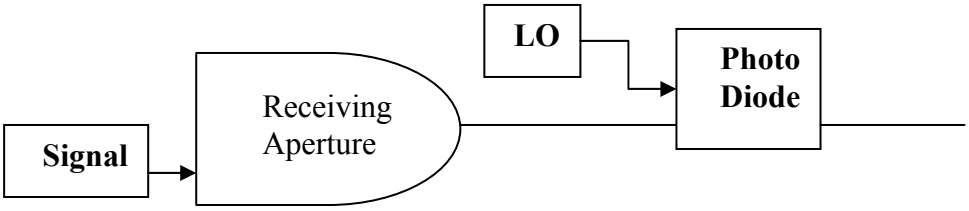

Fig. (3-2):Diagram showing the addition of the Lo [ ].

Since the detection process includes a local oscillator, the expression for the signal current out of the photo diode changes. For the coherent detection scheme, the output current is as follows [58]:

$$i_{sig} = \Re(\overrightarrow{E_r} + \overrightarrow{E_{lo}})^2 = \Re(\overrightarrow{E_r} + \overrightarrow{E_{lo}} + 2\overrightarrow{E_r} \bullet \overrightarrow{E_{lo}}) \quad (3\text{-}15)$$

where

E_{lo} = electric field vector due to the local oscillator

E_r = electric field vector due to the received signal

The expression for output current in terms of power instead of electric fields would be:

$$i_{sig} = \Re P_r + \Re P_{lo} + 2\Re\sqrt{P_r P_{lo}} \cos(\gamma/2)\cos[(\omega_{sig} - \omega_{lo})t + \varphi] \quad (3\text{-}16)$$

where

ω_{sig} = signal frequency [radians/s]

ω_{lo} = local oscillator frequency [radians/s]

φ = phase difference between signal and LO [radians]

P_{lo} = local oscillator power [W]

γ = polarization difference between received signal and LO

The expression above contains three terms. Only the third one is of interest for a coherent detection scheme. The first term is from direct detection and it appears at base band. It is at a part of the spectrum that is outside the frequency range of interest and is filtered out. The second term appears at DC. The third term appears at a frequency $\omega_{if} = \omega_{sig} - \omega_{lo}$ and it contains the multiplication of the signal and the LO terms. It is this multiplication that is desired from coherent detection, and the signals outside the desired part of the spectrum are filtered out. So, only looking at the term of interest gives the following expression for the i_{sig}:

$$i_{sig} = \Re\sqrt{P_r P_{lo}} \cos(\gamma/2)\cos[(\omega_{sig} - \omega_{lo})t + \varphi] \quad (3\text{-}17)$$

The desired cross term is the multiplication of the electric fields of the signal and the local oscillator, which gives the following simplified expression:

$$i_{sig} = 2\Re(E_r \bullet E_{1o}) \quad (3\text{-}18)$$

This is equivalent to the expression obtained from (3-17). (The use of dot product is necessary to account for the polarization difference between the signal and the LO).To obtain the maximum value for the output signal current, the value for γ is optimized. This term is included in equation (3-17) to account for the polarization difference between the signal and local oscillator electric fields. This polarization difference accounts for the degree of copolarization of the two signals. When they are not copolarized, the obtained signal power decreases. As seen from equation (3-17), the local oscillator power affects the signal current and, in turn, signal power, Psig. The SNR equation for coherent detection is as follows [59]:

$$SNR_{coh} = \frac{\Re^2 P_{lo} P_r}{P_{n-th} + P_{n-sh}} \tag{3-19}$$

Now that an expression for SNR for coherent detection is obtained, one can look at a numerical example in order to see the improvement in SNR compared to the incoherent detection system.

If P_{LO} = 1 mW and all other parameter values are same as they were for the incoherent detection scheme, the new value for electrical signal power, P_{sig}, is 8.10 $\times 10^{-17}$ W, an improvement of about 98 dB. The noise term also increases, however, due to the increase of shot noise. Shot noise is higher since $I_{incident}$ is higher. The increase of $I_{incident}$ is due to the contribution from the local current. The new shot noise value is2.56×10^{-13} W, while the value for the thermal noise power stays same at, $P_{n\text{-}th}$, is 2.26×10^{-13} W. This new value for signal power and the total noise power of 4.82×10^{-13} W gives an SNR of about –38 dB. This is an improvement of 94 dB compared to incoherent detection. With this improvement, one

will need an increase of 48 dB of signal power to obtain the necessary range accuracy for this system.

3.5 Pulse Compression:

Pulse compression is a technique widely used in radar systems to improve sensitivity. In this case the pulse compression process has a long-duration pulse, low peak-power, modulated transmit waveform to attain the detection and range resolution comparable to that of a short-pulse, high-peak-power system. One pulse compression method uses chirped signals. A chirp pulse compressed system has a sinusoidal pulse with a long duration, T, and an instantaneous frequency varying linearly with time. In other words, the pulse used is a chirp-modulated signal. Figure (3-3) below illustrates this concept [60].

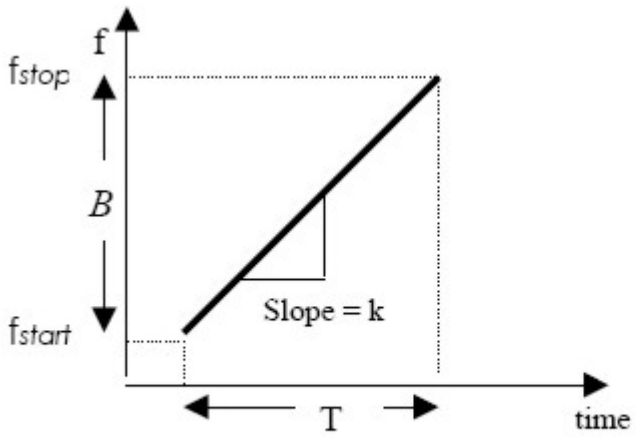

Fig. (3-3) Illustration of the concept of using a chirp signal

The slope of the line, k, is known as the chirp rate and is the ratio of the system bandwidth, B, to the system pulsewidth, T. The following expression is a mathematical description of the chirp signal:

$$S_{chirp} = A_c \sin(2\pi(f_{start}t + \frac{k}{2}t^2 + \varphi_{st})) for 0 \le t \le T \qquad (3\text{-}20)$$

where

A_c = amplitude of the chirp [V]

f start = starting frequency of the chirp [Hz]

φ_{st} = starting phase of the waveform [radians]

This chirp signal is used to amplitude modulate the transmitted signal. The following expression gives a mathematical description of the chirp-modulated signal:

$$S_{tx} = A_{tx}(1 + \mu S_{chirp})\sin(2\pi f_{car} t + \varphi_{optical}) \quad (3\text{-}21)$$

where

A_{tx} = amplitude of the transmitted signal [V]

μ = modulation index

f_{car} = carrier frequency [Hz]

$\varphi_{optical}$ = phase of the optical signal [radians]

The range for the modulation index is between 0 and 1. In this case, a value close to 1 is chosen to ensure maximum power transmission.

After the signal is transmitted, it reaches the target and is backscattered. A portion of this backscattered signal, S_{rx}, is captured at the receiving aperture of the system [60]. The following figure shows a graphical description of the received signal.

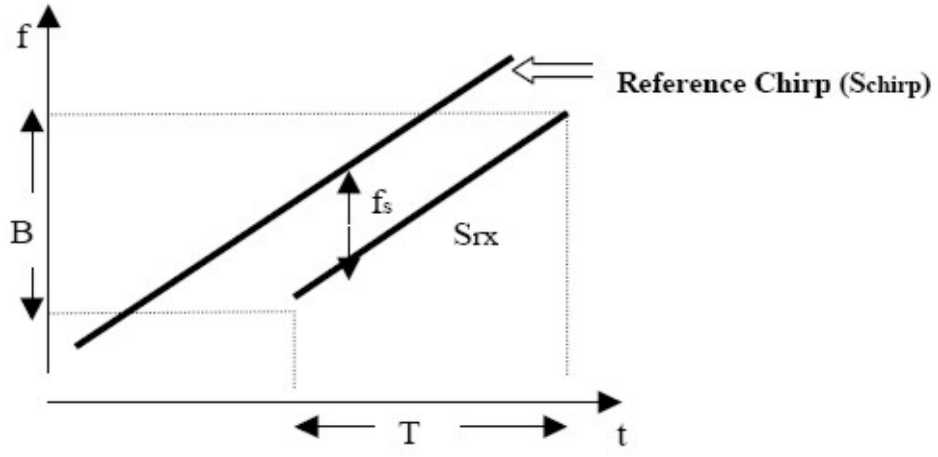

Fig. (3-4) Graphical representation of refrence and received signal

This received signal is shown in figure (3-4) as signal S_{rx}. The difference in frequency between S_{rx} and the reference chirp, f_s, is the frequency that gives the range to the target. After several processing steps, the received signal is multiplied with the S_{chirp}. This multiplication is called dechirping [61,62]. After dechirping, low-pass filter the dechirped signal to obtain the frequency of interest, f_s. Once we have the frequency, f_s, we can determine the range. The range to the target can be obtained from the following formula:

$$R = \frac{f_s c}{2k} \tag{3-22}$$

This relationship also forms the basis of the formula to be used to find the range resolution of our system. Range resolution is a parameter that gives the minimum range separation two targets can have and still be resolved as two distinct targets. It is dependent on the pulse length of our system, T. The range resolution, ΔR , can be obtained from the following formula:

$$\Delta R = \frac{c}{2kT} \tag{3-23}$$

This relationship is still bandwidth dependent since $k\ T = B = 1/\tau$. The term τ is the duration of the pulse after compression. The ΔR obtained for this system is the same as the one obtained from a short-pulse system of duration τ . Pulse compression is used to obtain a signal processing gain and improve the SNR. The amount of compression gain obtained from the system is seen from the *pulse compression ratio,* which is simply the ratio of the transmitted pulse duration, T, to the system's effective pulse duration, τ and is given by [58]:

$$CR = T/\tau \tag{3-24}$$

The effective pulse duration, $\tau = 1/B$, where B is the chirp bandwidth. For this system B = 260 MHz and T = 40 μs , which gives a chirp rate of k = 6.5 MHz/ μs. ΔR for this system is 0.576 m. These values give a compression gain of about 40 dB. When this gain is applied to the SNR of –38 dB obtained previously, the SNR increases to about 2 dB. At this point the SNR needs further improvement for detection.

3.6 Coherent Integration:

When the modulated pulse is transmitted, it reaches the target and is backscattered. A portion of the backscattered signal reaches the receiver, is processed, and then digitized. This signal is a sinusoid, which is buried in noise. This process is repeated for each transmitted signal. The phase and frequency are the same for each pulse. The noise in the received signals, however, is random and is different for each pulse. If the received sinusoids are added together, the sinusoid part will add constructively while the noise will add destructively, because noise is uncorrelated. As the received signals are averaged together, the signal power will stay the same while the noise power level will be reduced, yielding an improved SNR. The following expression gives the mathematical formula for this averaging called coherent integration [58].

$$S_{rx(n)} = \frac{1}{N}\sum_{n}^{N} S_{rs}(n) \qquad \text{for n = 1, 2, .., N} \tag{3-25}$$

where

N = number of signals averaged

The signal processing gain obtained from the averaging is N. So, if 10 coherent integrations are performed, the SNR will be improved by 10 dB. However, one should keep in his mind that this process has its limits for improving SNR. This limit is due to nonrandom system noise dominating

the noise term when the noise floor is reduced to a certain limit. Since this noise source is not random, the averaging does not reduce the noise floor and the SNR is not improved. Increasing the number of coherent integrations also increases the sampling area of the target. This is due to the fact that the radar is moving and the target is stationary. For this case, only need about 10 dB of SNR improvement for target detection, which is well within the limits of this process. When the 10 dB improvement is added to the SNR of 2 dB obtained after pulse compression, one get an SNR of 12 dB. Then one can make sure that an SNR of 12 dB is enough to get a range accuracy of 10 cm. For a pulse bandwidth of 260 MHz and an SNR of 12 dB, from equation (3-1) predicts a range accuracy of 10.3 cm, which meets the science requirement.

Chapter Four

Mathmatical Modeling of the System

4.1 Introduction:

This chapter presents the system design that would achieve the performance described in Chapter 3, and the mathematical representations for signals produced at different sections of the system to better understand how everything works.

4.2 System Block Diagram:

In this section, the block diagram is presented to explain the system design. Figure (4-1) shows this block diagram that will be used to implement the concepts presented in Chapter 2. It has three main subsections: the transmitter, the receiver and the signal processing sections. The transmitting and receiving subsections have both optical and RF parts [51].

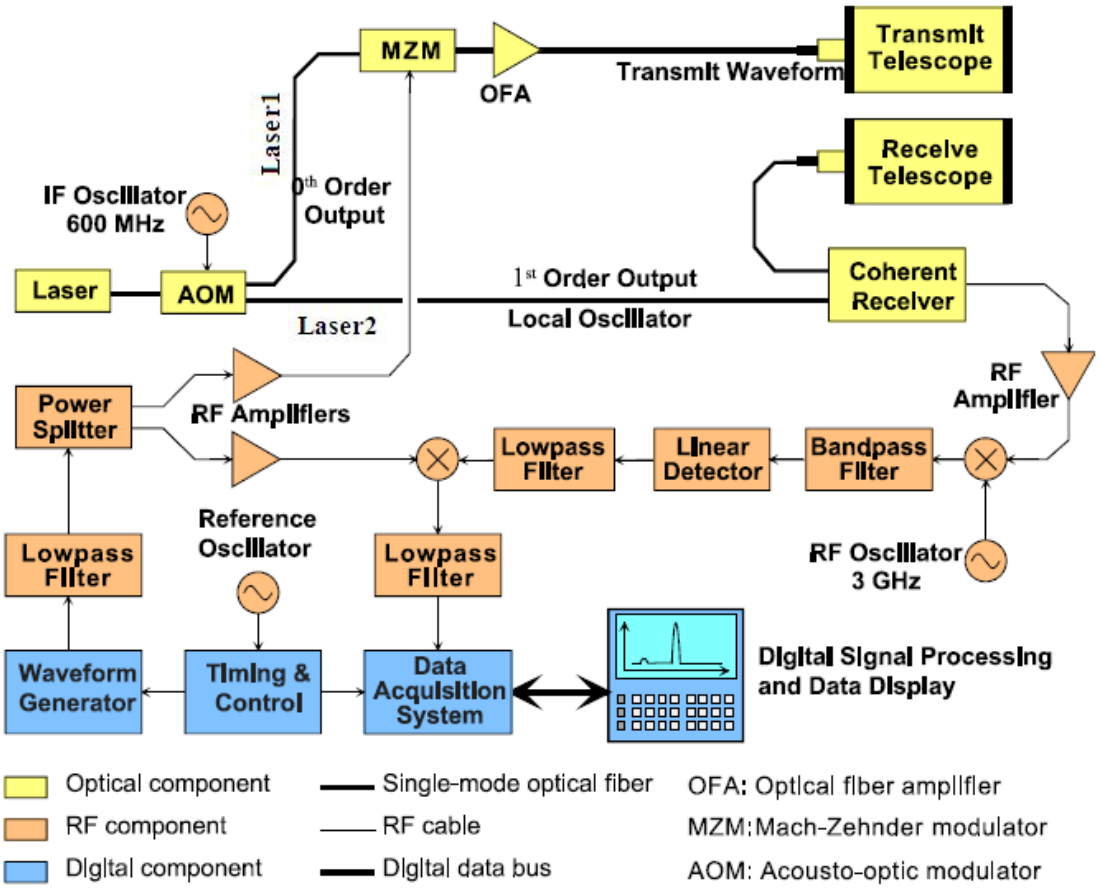

Fig. (4-1): The hybrid RF/laser radar block diagram [51]

4.2-1 The Transmitter:

The transmitter of the system consists of a waveform generator, RF components including a 600 MHz oscillator, a low-pass filter, a power splitter, and an RF amplifier and optical components including a 1319 nm wavelength laser source, an acousto-optic modulator (AOM), a Mach-Zehnder modulator (MZM), optical fiber amplifier (OFA) and a transmit telescope.

4.2-1-1 The Waveform Generator:

The waveform generator is used to generate a chirp signal with a bandwidth of 260 MHz and a duration of 40 μs . The start frequency of the chirp is 100 MHz and the stop frequency is 360 MHz. This chirp signal is generated every 100 μs giving a 40% duty cycle.

4.2-1-2 The RF Section of the Transmitter:

This section of the transmitter includes a 600 MHz oscillator, a low-pass filter, a power splitter and an RF amplifier.

a) Oscillator: The oscillator outputs a 600 MHz signal, and this signal drives the AOM, which serves as a frequency shifter. This frequency-shifted light is the local oscillator signal that is input to the coherent receiver.

b) Low-pass Filter: The low-pass filter is used to block high frequency signals coming out of the waveform generator before they enter the power splitter. It has a cut-off frequency of 450 MHz and is used to filter out any harmonics or unwanted signals that might be produced during wave generation.

c) Power Splitter: The power splitter is used to split the incoming signal into two signals. One of those signals is used to drive the Mach-Zehnder

modulator (MZM). The other output is used in the receiver section to dechirp the detected signal.

d) RF Amplifier: The RF amplifier is used to amplify the signal coming out of the power splitter before it is used to drive the MZM.

4-2-1-3 The Optical Section of the Transmitter:

This section of the transmitter includes a 1319 nm wavelength laser source, an acousto-optic modulator (AOM), a Mach-Zehnder modulator (MZM), optical fiber amplifier (OFA) and a transmit telescope.

a) Laser Source: The laser source produces CW light at 1319 nm and has a maximum power output of 20 dBm and a spectral width of 5 kHz. This light is then passed through the AOM and is modulated at the MZM.

b) Acousto-optic Modulator: The AOM is placed after the laser source and is used to split the incoming light into two paths: the 0^{th} order port path and the 1^{st} order port path. The light directed to the 0^{th} order port path (the path for the unshifted light) is the input to the MZM, while the frequency of the light directed to the 1^{st} order port path is shifted down by 600 MHz. This light is then input to the coherent receiver.

c) Mach-Zehnder Modulator: The MZM takes the CW 1319 nm optical signal and intensity modulates it with the chirp waveform.

d) Optical-fiber Amplifier: The OFA is used to amplify the optical signal coming out of the MZM. The gain obtained from this OFA is about 23 dB.

e) Transmit Telescope: The optical tool used to transmit the optical signal is a telescope. Instead of the eyepiece used for traditional telescope applications, a fiber interface is mounted at the back of the telescope. This interface is used to launch light into the telescope through its optics. The telescope has an aperture with a diameter of 127 mm, a focal length of 1.27 m, and an aperture blockage diameter of 0.085 m.

4.2-2 The Receiver:

The receiver of the system consists of a receive telescope, a coherent receiver, two RF amplifiers, two RF mixers, a 3 GHz RF oscillator, a band-pass filter, an envelope detector, and two low-pass filters.

4.2-2 -1 The Optical Section of the Receiver:

This section of the receiver includes the receive telescope and the coherent receiver.

a) Receive Telescope: The aperture used to receive the light scattered from the target is the same type of telescope described above in the transmitter section. The only difference is in the direction of light, which is from the receiving aperture, through the fiber interface, to the fiber leading to the coherent receiver.

***b) Coherent Receiver*:** The coherent receiver is used to achieve coherent detection of the optical signal scattered from the target. The receiver has two inputs: 1) the light captured by the receive aperture and 2) the light from the AOM that has a frequency shift of 600 MHz with respect to the original optical signal. This frequency-shifted light is called the local oscillator signal and will be used to boost the detected signal power by coherent detection. These two optical signals are mixed and the output of the coherent receiver is a RF signal. (The photo detector used in this configuration has a noise equivalent power (NEP) of 24 pA / Hz **.**)

4.2-2 -2 The RF Section of the Receiver:

This section of the receiver includes two RF amplifiers, a 3 GHz RF oscillator, two RF mixers, a bandpass filter, an envelope detector and two low-pass filters.

a) RF Amplifiers: The first of the RF amplifiers is placed after the coherent receiver and it boosts the signal power of its output. It provides an amplification of 30 dB, has a noise figure of 5.5 dB and a bandwidth

from 50 MHz to 1 GHz. The second RF amplifier is used to boost the signal power of the signal coming out of the second port of the power splitter. It provides an amplification of 15 dB, has a noise figure of 6 dB and a bandwidth from 10 MHz to 4.2 GHz.

b) 3 GHz Oscillator: The oscillator used in the receiver section produces a 3 GHz signal. Its output is fed into the first mixer to increase the frequency of the signal at its input.

c) RF Mixers: The first of the RF mixers takes the output of the coherent receiver and upconverts it by 3 GHz using the RF oscillator as its second input. Its output has a frequency 3 GHz higher than the output of the coherent receiver. This is done to provide optimum detection for the envelope detector as it requires a 10:1 or higher ratio between the carrier and envelope frequencies. The second mixer is used to mix the low-pass-filtered output of the envelope detector and the original chirp signal to produce a dechirped signal at its output.

d) Bandpass Filter: The bandpass filter placed after the RF mixer is included in the receiver configuration to filter out any unwanted harmonics or signals that may be produced during the up conversion of the signal in the previous mixing operation. It has a center frequency of 3.5 GHz and a bandwidth of 1 GHz.

e) Envelope Detector: The envelope detector has the up-converted signal at its input port as it is used to detect the envelope of this signal. The information about the target's range is obtained from the envelope of this signal, and the frequency information leading to this range information is obtained after dechirping and signal processing. The envelope of the signal is obtained after low-pass filtering the output of the envelope detector, which is discussed below.

f) Low-Pass Filters: The first of the low-pass filters (LPF) is placed after the envelope detector to obtain the envelope of its input signal. High-

frequency terms produced during the envelope detection process are low-pass filtered to obtain the envelope. The second LPF is placed in the path of the dechirped signal to filter out any unwanted signals. The first LPF has a cutoff frequency of 467 MHz while the second one has a cutoff of 10.7 MHz.

4.3 Mathmatical Modeling of the System:

In this section, mathematical representations for signals produced at different sections of the system are presented to better understand how everything works. The block diagram as shown in figure (4-1) has two optical signals shown to be outputs from laser1 and laser2. Laser2 outputs light that is intensity modulated to get the transmit signal. It is intensity modulated with a chirp signal, m(t), produced by the waveform generator.

The expression for m(t) is given below:

$$m(t) = a\cos(2\pi f_c t + 0.5kt^2 + \phi_c) \tag{4-1}$$

where

m(t) = the chirp waveform [V]

f_c = the chirp start frequency [Hz]

k = the chirp rate [s^{-2}]

a = the modulation index of the chirp waveform ($0 < a \leq 1$)

ϕ_c = the chirp start phase [radians]

After the optical signal is intensity modulated, it is transmitted. This signal is labeled as q(t) and is expressed as follows:

$$q(t) = \frac{A}{2}[1 + m(t)]\cos(2\pi f_{TX} t + \phi_{TX}) \tag{4-2}$$

where

q(t) = transmit signal [V]

A = amplitude of the transmitted signal [V]

f_{TX} = optical frequency of the transmit signal [Hz]

ϕ_{TX} = phase of the optical transmitted signal [radians]

This signal received from the target, r(t), reaches the receiving aperture of the system and is captured. The expression for r (t) (ignoring effects of frequency instability and Doppler) is as follows:

$$r(t) = \frac{A\alpha}{2}[1 + m(t-\tau)]\cos[2\pi f_{TX}(t-\tau) + \phi_{RX}] \qquad (4\text{-}3)$$

where

r(t) = received signal [V]

α = round-trip loss factor ($0 < \alpha < 1$)

ϕ_{RX} = phase of the received signal [radians]

τ = round-trip signal travel time [s]

This signal then goes through the coherent detection process. As explained in Chapter 2, this process requires a local oscillator LO signal. This signal, p (t), is supplied here by laser 1. The frequency of this signal differs from that of laser 2 by f_s.

The expression for the LO signal is:

$$p(t) = \cos[2\pi(f_{TX} + f_S)t + \varphi_{LO}] \qquad (4\text{-}4)$$

where

p(t) = local oscillator signal [V]

f_s = frequency shift of the LO signal [Hz]

φ_{LO} = starting phase of the LO signal [radians]

Figure (4-2) shows the signals mentioned up to this point in frequency domain and is presented below for better understanding of the system.

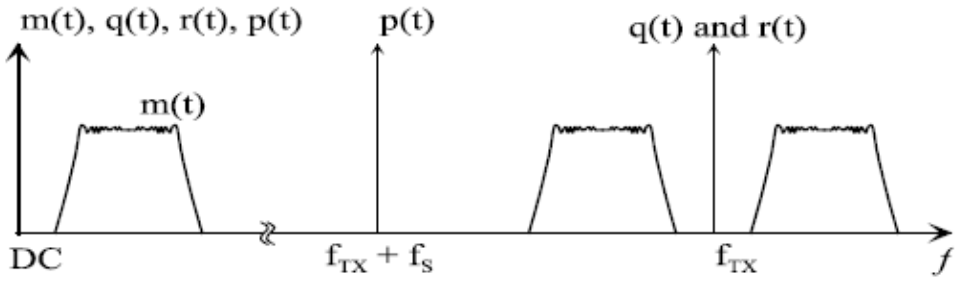

Fig. (4-2): Signal of interest in frequency domain

During the detection process, thermal and shot noise with bandwidth BR are introduced to the system. These are assumed to be the only noise sources in the system. This noise term is n(t) and its expression is given below:

$$n(t) = n_o\{\cos[\theta_n(t)] + j\sin[\theta_n(t)]\} \tag{4-5}$$

where

n_o = noise term [V]

θ_n (t) = random phase that follows a uniform distribution [radians]

The signal from the coherent receiver is s(t) + n(t), where s(t) denotes the result of square-law detection of the return signal r(t) with the LO signal p(t). The expression for s(t) is given below:

$$s(t) = \Re[r(t) + p(t)]^2 \tag{4-6}$$

where

s(t) = detected signal [V]

$\Re$ = photodiode responsivity [A/W]

$$s(t) = \Re\{\ \frac{A\alpha}{2}[1 + m(t-\tau)]\cos[\pi f_{TX}(t-\tau) + \phi_{RX}]\cos^2[2\pi(f_{TX} + f_s)t + \phi_{lo}]\}^2$$

$$s(t) = \Re\{(A\alpha/2)^2[1 + m(t-\tau)]^2\cos^2[2\pi f_{TX}(t-\tau) + \phi_{RX}] + \cos^2[2\pi(f_{TX} + f_s)t + \phi_{RX}]$$
$$A\alpha[1 + m(t-\tau)]\cos[2\pi f_{TX}(t-\tau) + \phi_{RX}]\cos[2\pi(f_{TX} + f_s)t + \phi_{lo}]$$

$$s(t) = \frac{\Re}{2}\{A\alpha/2)^2[1 + 2m(t-\tau) + m^2(t-\tau)]\{1 + \cos[2\pi 2 f_{TX}(t-\tau)2 + \phi_{RX}]\}$$
$$+ \{1 + \cos[2\pi(f_{TX} + f_s)t + 2\phi_{LO}]\}$$
$$+ Aa[1 + m(t-\tau]\{\cos(-2\pi f_s t - 2\pi f_{TX}\tau + \phi_{RX} - \phi_{LO})$$
$$+ \cos[2\pi f_{TX}(t-\tau)\{+\phi_{RX} + 2\pi(f_{TX} + f_s)t + \phi_{LO}]\}$$
$$+ \cos[2\pi f_{TX}(2t-\tau) + \phi_{RX} + \phi_l]\}$$
$$+ \cos[2\pi f_{TX}(2t-\tau) + \phi_{RX} + \phi_l]\}$$

Since optical signals and harmonics of optical signals are suppressed, this expression reduces to:

$$s(t) = \frac{\Re}{2}[(A_a/2)^2[1 + 2m(t-\tau) + m(t-\tau)^2] + 1 + A\alpha[1 + m(t-\tau)]\cos(-2\pi f_s t - 2\pi f_{TX}\tau + \phi_{RX} - \phi_{LO})]$$

To obtain the total coherent receiver output, the noise term n (t) should be added as shown below:

$$S(t) + n(t) = \frac{\Re}{2}[\{A\alpha/2\}^2[1 + m(t-\tau) + m^2(t-\tau)] + 1$$
$$+ A\alpha[1 + m(t-\tau)]\cos(-2\pi f_s t - 2\pi f_{TX}\tau + \phi_{Rx} - \phi_{LO})] + n(t) \qquad (4\text{-}7)$$

This signal is then passed through a bandpass filter of bandwidth B1. This filter rejects the DC and double frequency terms together with the baseband chirp and chirp-squared terms, and the following expression is obtained:

$$u(t) = \frac{\Re A\alpha}{2}[1 + m(t-\tau)]\cos(-2\pi f_s t - 2\pi f_{TX}\tau + \phi_{RX} - \phi_{LO}) + n(t)\frac{B_1}{B_R} \qquad (4\text{-}8)$$

where

u(t) = output of the first bandpass filter [V]

B_1 = bandwidth of the first bandpass filter [Hz]

B_R = receiver bandwidth [Hz]

Figure(4-3) shows the baseband chirp and chirp-squared terms, which are rejected by the bandpass filter, in addition to the terms inside the passband.

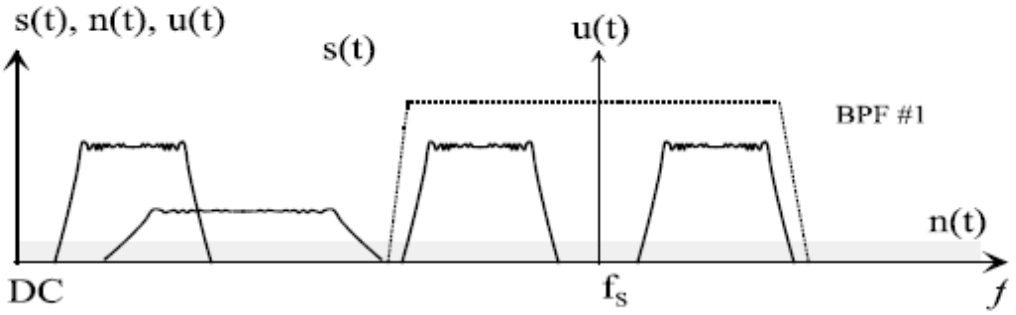

Fig. (4-3) The various signal in the system.

The output of the bandpass filter is then fed to the linear detector to obtain the signal of interest from the envelope of u(t). The output of this square-law detection process is v(t) and the expression of v(t) is given below:

$$v(t) = \eta[u(t)]^2 \tag{4-9}$$

$$V(t) = \eta\{\frac{\Re A_a}{2}[1 + m(t-\tau)]\cos(-2\pi f_s t_{TX}\tau + \phi_{RX} - \phi_{LO}) + n(t)\frac{B_1}{B_2}\}^2$$

$$v(t) = \eta\{\frac{\Re A\alpha}{2}[1 + m(t-\tau)]\cos(2\pi f_s t - 2\pi f_{TX}\tau + \phi_{RX} - \phi_{LO})\}^2$$

$$+ \eta\Re Aa[1 + m(t-\tau)]\cos(2\pi f_s t - 2\pi f_{TX}\tau + \phi_{RX} - \phi_{LO})n(t)\frac{B_1}{B_R} + \eta n^2(t)(\frac{B_1}{B_R})^2$$

$$v(t) = \eta\left(\frac{\Re A\alpha}{2}\right)^2 [1 + m(t-\tau)]^2 \cos^2(2\pi f_s t - 2\pi f_{TX}\tau + \phi_{RX} - \phi_{LO})$$

$$+ \eta\Re\alpha[1 + m(t-\tau)]\cos(2\pi f_s t - 2\pi f_{TX}\tau + \phi_{RX} - \phi_{LO})n(t)\frac{B_1}{B_R} + \eta n^2(t)\left(\frac{B_1}{B_R}\right)^2$$

where

v(t) = output of the linear detector [V]

η = detector efficiency ($0<\eta<1$)

The output of the linear detector is then passed though a second bandpass filter to reject DC, double-chirp, and IF terms. The expression for its output is given below:

$$W(t) = \eta(\frac{\Re A_a}{2})_2 m(t-\tau) + \eta\Re Aan(t)\frac{B_1}{B_R}\eta n^2(t)\left(\frac{B_1}{B_R}\right)^2 \quad (4\text{-}10)$$

$$W(t) = \eta\left(\frac{\Re A\alpha}{2}\right)^2 m(t-\tau) + \eta\Re A\alpha n(t)\frac{B_1}{B_R} + \eta n^2(t)\left(\frac{B_1}{B_R}\right)^2 \quad (4\text{-}11)$$

where

w(t) = output of the second bandpass filter [V]

The signal w(t) is then mixed with the original chirp signal to obtain the dechirped signal x(t). Its expression is shown below:

$$x(t) = m(t)[\eta(\frac{\Re A\alpha}{2})^2 m(t-\tau) + \eta\Re An(t)\frac{B_1}{B_R}\eta n^2(t)\left(\frac{B_1}{B_R}\right)^2] \quad (4\text{-}12)$$

where

x(t) = dechirped signal [V]

In order to understand how the signal that is input to the signal processor, y(t), is obtained, the following analysis of dechirping is presented. It

shows the original chirp signal, m(t), mixed with the chirp signal that has a time delay, τ , due to its travel time to the target.

$$m(t)m(t-\tau) = a\cos(2\pi f_c t + 0.5kt^2 + \phi_c)a\cos[2\pi f_c(t-\tau) + 0.5k(t-\tau)^2 \_ \phi_c]$$

$$m(t)m(t-\tau) = \frac{a^2}{2}[\cos(2\pi f_c + kt\tau - 0.5k\tau^2)\cos(2\pi 2 f_c t - 2\pi f_c \tau + kt^2 - k\tau t + 0.5k\tau^2 + 2\phi_c)]$$

Of the terms seen above, the cosine term with $2\pi f_C \tau$ has the target range information. When this product is low-pass filtered, the following expression is obtained, which contains the signal of interest:

$$y(t) = \frac{\eta(\Re A\alpha a)^2}{8}\cos(2\pi f_c\tau + kt\tau - 0.5k\tau^2)$$
$$+ \eta\Re A\alpha m(t)n(t)\left(\frac{B_1}{B_R}\right) + \eta n^2(t)\left(\frac{B_1}{B_R}\right)^2 m(t)$$

where

y(t) = signal to be processed [V]

When y(t) is obtained, it is input to the signal processor. The signal processor performs the FFT to obtain the frequency domain representation of the signal. When the spectrum of the signal is at hand, all the parts except for the part containing the signal is filtered out. This is done to reject noise and any other undesired signals. The following section explains the processes in the signal processing section.

4.4 Signal Processing:

During the signal processing section of the detection process, the spectrum of the signal is obtained by performing an FFT on y(t). The length of the FFT is fixed since the signal has fixed pulsewidth. This limited pulse width restricts the time to collect data and take FFT. Hence,

the bin width of the FFT is fixed. Once the FFT is performed, the unwanted parts of the incoming signal are filtered out to obtain the signal of interest. Coherent integrations are performed to improve the SNR. The premise behind coherent integration is explained in Chapter 2 in detail, but the general idea is to improve SNR by reducing random noise level. Since the signal of interest is not random, this process does not affect it.

The expression SNR per bin is shown below. This is easily obtained since noise and signal per bin are known and SNR per bin is found by taking the ratio of signal per bin to noise per bin.

$$SNRperbin = \frac{\frac{\eta(\Re A\alpha a)^2}{8}\cos(2\pi f_c\tau + kt\tau - 0.5k\tau^2)}{\eta\Re A\alpha m(t)n(t)\left(\frac{B_1}{B_R}\right) + \eta n^2(t)\left(\frac{B_1}{B_R}\right)^2 m(t)} \tag{4-12}$$

The numerator represents the signal while the denominator represents the noise. The first term in the denominator contains the n(t) term, which has a Gaussian distribution and is reduced. Once the signal is easily observed in the spectrum, its frequency is obtained. This frequency information is then used to obtain the range to the target using the following formula:

$$Rangetot\arg et = \frac{(signalfrequency)(speedoflight)}{(chirprate)} \tag{4-13}$$

while this expression provides the range information, the range accuracy can be obtained from the SNR information using equation (3-1).

Chapter Five

Simulation of the System Using Matlab Package and Results

5.1 Introduction:

This chapter presents simulations done with Matlab (V. 7) to predict the behavior of the laser radar system under different conditions with different parameters. Simulations are carried out so that system performance can be predicted without the need to make changes in hardware. First presented is simulation of coherent detection, incoherent detection, and signal to noise ratio for coherent detection with respect to local power. Secondly a block diagram containing each steps of the simulation of the receiver. Also presented are the values of the parameters used and their variable names used in the program. Next is the presentation of simulation results obtained by changing selected parameters and seeing their effect on target detection. To help explaining the results better they are given in tables or graphs or both.

5.2 Receiver—Simulation and results:

Simulation is carried out in order to determine the shot-noise (P_{n_sh}) characteristics and how the receiver will behave for a shot-noise-limited system and thermal noise (P_{n_th}). Several assumptions were taken into consideration when the simulation was done. First, the bandwidth of the system is 800 MHz corresponding to the photoreceiver bandwidth. This sets the noise bandwidth. Secondly, the temperature of the system is assumed to be at constant room temperature (i.e., 290 K), and the responsivity, $\Re$, of the photoreceiver is assumed to be 1 A/W. The purpose of this simulation is to find out how the chang optical local oscillator power(Pwr_Lo) will affect the detected coherent return signal power (P_{coh}), direct detected signal power (P_{Incoh}), and noise at the coherent receiver output . Tables (5-1) to (5-4) summarize the most important parameters using equations (3-12), (3-13) and (3-14)). Figure

(5-1) to Figure (5-4) show that by increasing the optical local (Lo) power, the coherently detected signal increases as expected.

Table (5-1) The effect of Pwr_in on parameters(P_{n_th} , P_{n_sh}, P_{coh}, and P_{Incoh}) when Pwr_Lo = -20dBm.

N0.	Pwr_in (dBm)	P_{n_th} (dBm)	P_{n_sh} (dBm)	$P_{n\_th} + P_{n\_sh}$ (dBm)	P_{coh} (dBm)	P_{Incoh} (dBm)
1	-90	-123.36	-115.9	-115.19	-140	-240
2	-80	-123.36	-115.9	-115.19	-130	-220
3	-70	-123.36	-115.9	-115.19	-120	-200
4	-60	-123.36	-115.9	-115.19	-110	-180
5	-50	-123.36	-115.9	-115.19	-100	-160
6	-40	-123.36	-115.9	-115.19	-90	-140
7	-30	-123.36	-115.9	-115.19	-80	-120
8	-20	-123.36	-115.9	-115.19	-70	-100
9	-10	-123.36	-115.87	-115.16	-60	-80
10	0	-123.36	-115.5	-114.84	-50	-60
11	10	-123.36	-112.9	-112.53	-40	-40
12	20	-123.36	-105.5	-105.4	-30	-20
13	30	-123.36	-95.87	-95.86	-20	0
14	40	-123.36	-85.913	-85.9	-10	20

Table (5-2) The effect of Pwr_in on parameters(P_{n_th} , P_{n_sh}, P_{coh}, and P_{Incoh}) when Pwr_Lo = -10dBm.

N0.	Pwr_in (dBm)	Pn_th (dBm)	Pn_sh (dBm)	Pn_th+Pn_sh (dBm)	Pcoh. (dBm)	PIncoh (dBm)
1	-90	-123.36	-105.92	-105.8	-130	-240
2	-80	-123.36	-105.92	-105.8	-120	-220
3	-70	-123.36	-105.92	-105.8	-110	-200
4	-60	-123.36	-105.92	-105.8	-100	-180
5	-50	-123.36	-105.92	-105.8	-90	-160
6	-40	-123.36	-105.92	-105.8	-80	-140
7	-30	-123.36	-105.92	-105.8	-70	-120
8	-20	-123.36	-105.92	-105.8	-60	-100
9	-10	-123.36	-105.92	-105.8	-50	-80
10	0	-123.36	-105.87	-105.79	-40	-60
11	10	-123.36	-105.5	-105.4	-30	-40
12	20	-123.36	-102.9	-102.86	-20	-20
13	30	-123.36	-95.5	-95.49	-10	0
14	40	-123.36	-85.8	-85.87	0	20

Table (5-3) The effect of Pwr_in on parameters(P_{n_th} , P_{n_sh}, P_{coh}, and P_{Incoh}) when Pwr_Lo = 0 dBm.

N0.	Pwr_in (dBm)	Pn_th (dBm)	Pn_sh (dBm)	Pn_th+ Pn_sh (dBm)	Pcoh (dBm).	PIncoh (dBm)
1	-90	-123.36	-95.90	-95.90	-120	-240
2	-80	-123.36	-95.90	-95.90	-110	-220
3	-70	-123.36	-95.90	-95.90	-100	-200
4	-60	-123.36	-95.90	-95.90	-90	-180
5	-50	-123.36	-95.90	-95.90	-80	-160
6	-40	-123.36	-95.90	-95.90	-70	-140
7	-30	-123.36	-95.90	-95.90	-60	-120
8	-20	-123.36	-95.90	-95.90	-50	-100
9	-10	-123.36	-95.90	-95.90	-40	-80
10	0	-123.36	-95.90	-95.90	-30	-60
11	10	-123.36	-95.86	-95.86	-20	-40
12	20	-123.36	-95.5	-95.49	-10	-20
13	30	-123.36	-92.9	-92.9	0	0
14	40	-123.36	-85.5	-85.5	10	20

Table (5-4) The effect of Pwr_in on parameters(P_{n_th} , P_{n_sh}, P_{coh}, and P_{Incoh}) when Pwr_Lo = 10 dBm.

N0.	Pwr_in (dBm)	Pn_th (dBm)	Pn_sh (dBm)	Pn_th+ Pn_sh (dBm)	Pcoh. (dBm)	PIncoh (dBm)
1	-90	-123.36	-85.90	-85.90	-110	-240
2	-80	-123.36	-85.90	-85.90	-100	-220
3	-70	-123.36	-85.90	-85.90	-90	-200
4	-60	-123.36	-85.90	-85.90	-80	-180
5	-50	-123.36	-85.90	-85.90	-70	-160
6	-40	-123.36	-85.90	-85.90	-60	-140
7	-30	-123.36	-85.90	-85.90	-50	-120
8	-20	-123.36	-85.90	-85.90	-40	-100
9	-10	-123.36	-85.90	-85.90	-30	-80
10	0	-123.36	-85.90	-85.90	-20	-60
11	10	-123.36	-85.90	-85.90	-10	-40
12	20	-123.36	-85.87	-85.87	0	-20
13	30	-123.36	-85.50	-85.50	10	0
14	40	-123.36	-82.90	-82.90	20	20

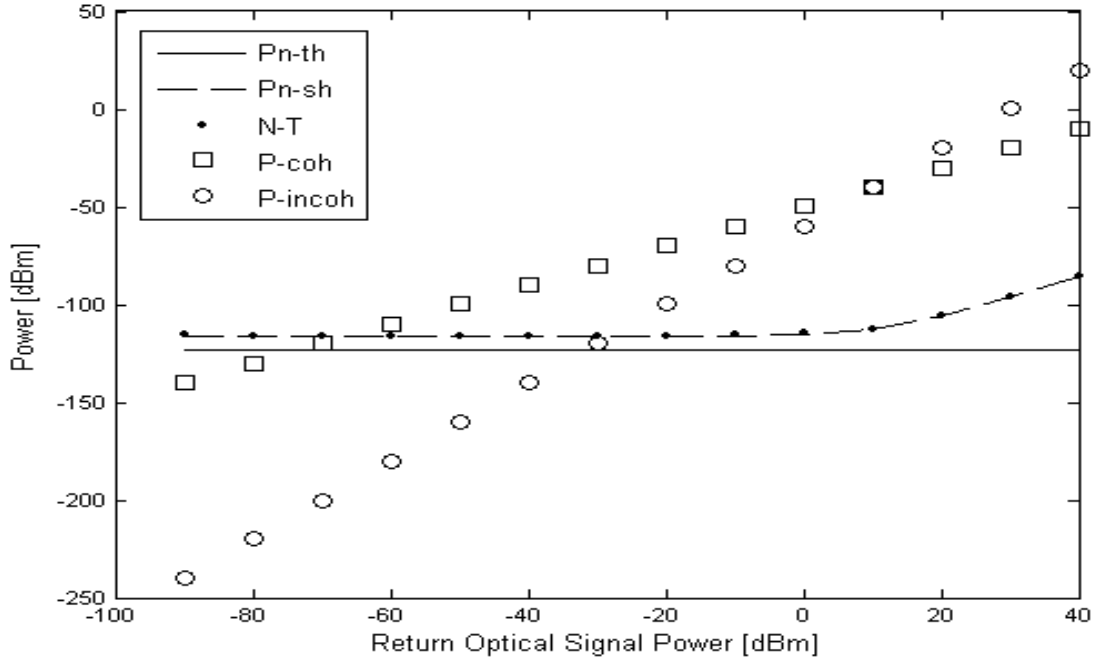

Fig. (5-1) Variation with return signal power: -20 dBm optical LO power.

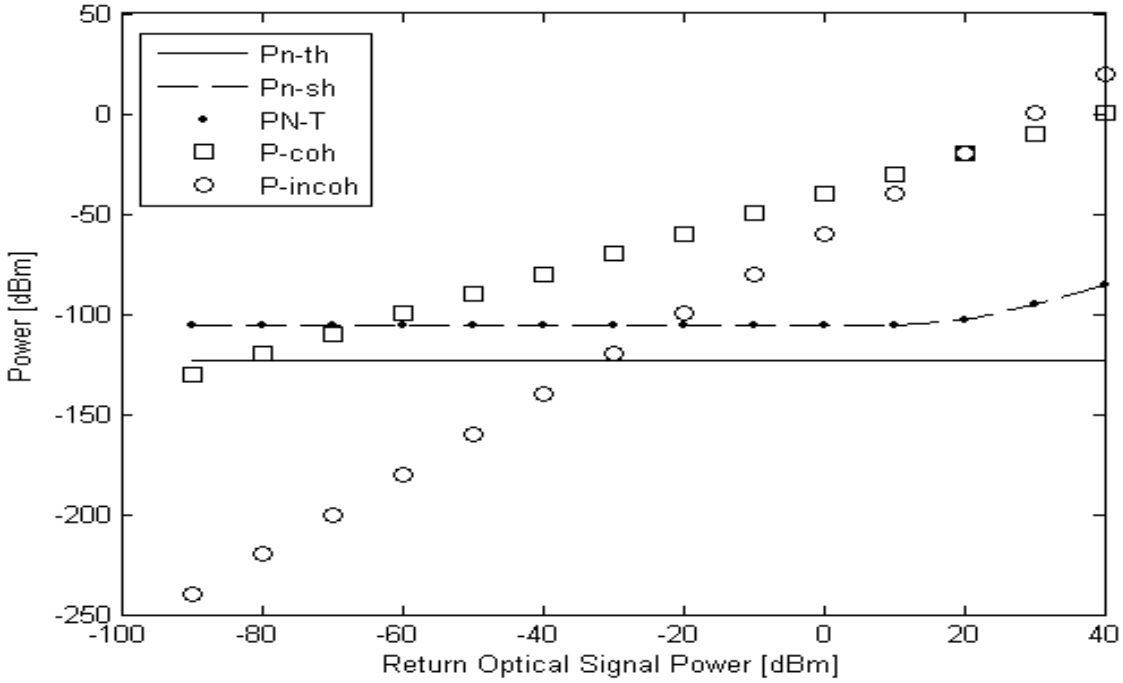

Fig. (5-2) Variation with return signal power: -10 dBm optical LO power.

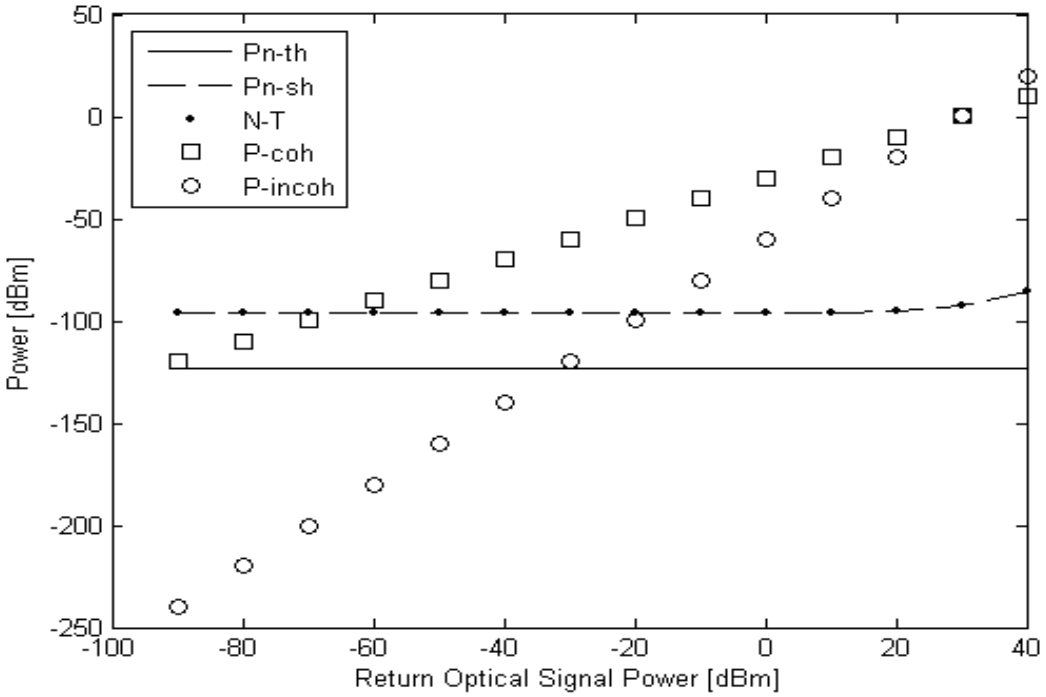

Fig. (5-3) Variation with return signal power: 0 dBm optical LO power.

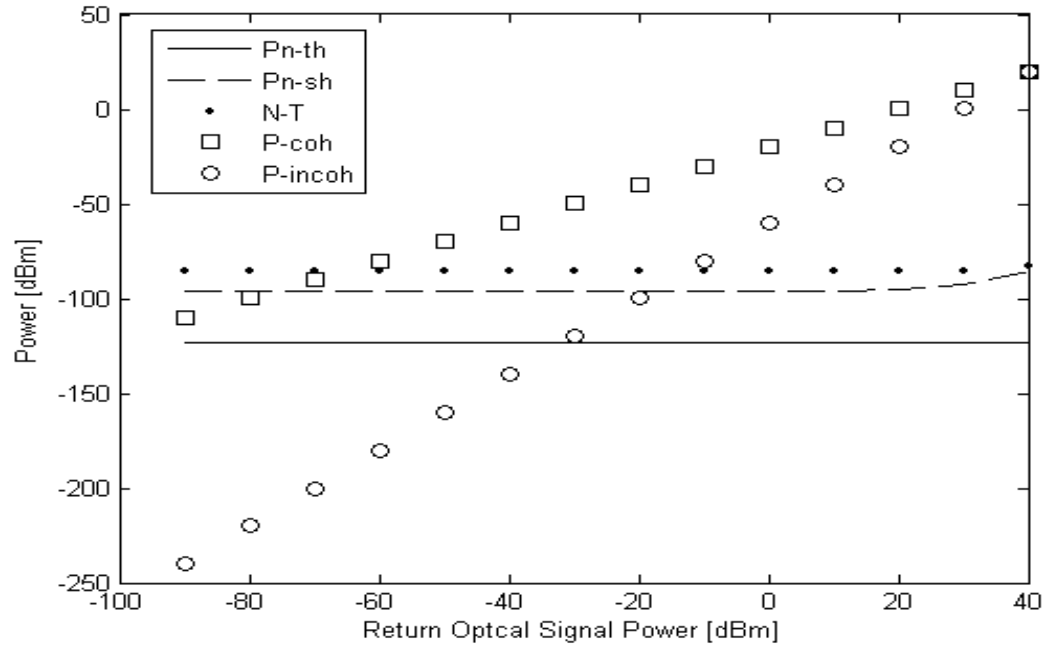

Fig. (5-4) Variation with return signal power: 10 dBm optical LO power.

One can notice that the crossing point between the directly detected signal curve and the coherently detected signal increases with respect to

increasing optical LO power. However, only the coherently detected signal is useful., the coherently detected signal power is much higher than a directly detected signal. Taking into consideration that the return signal will be very weak, and that the direct detected signal should be as weak as possible in comparison to the coherently detected signal, a suitable optical LO power should be chosen. Figure (5-1) to Figure (5-4) show that the optical LO power should be as high as possible.

A similar simulation was done to determine how much optical local power to be used. The relationship between SNR at the photodetector output and the local power for a fixed return signal of –90 dBm and 800 MHz photodetector bandwidth is given in Figure (5-5).

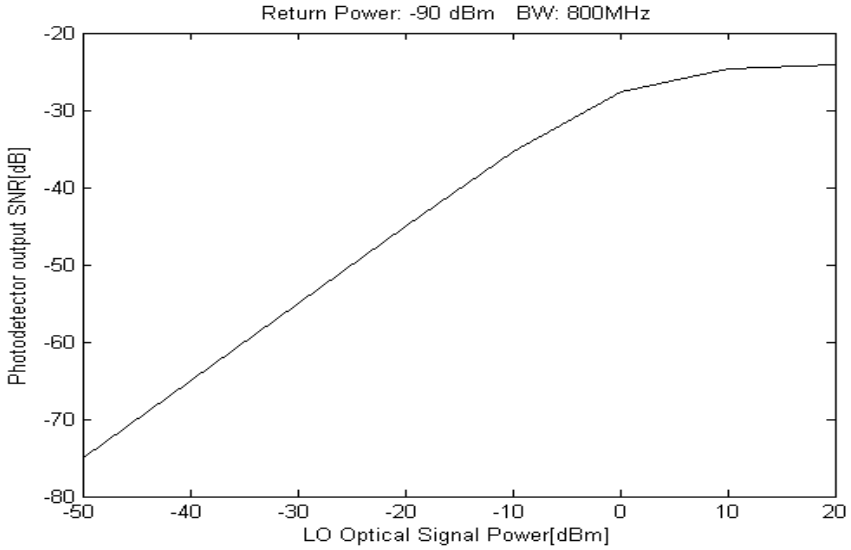

Fig. (5-5) Photodetector output SNR and optical LO power relationship.

The relationship in Figure (5-5) shows that the SNR does not improve beyond using 0 dBm of optical Lo power. This puts a limitation on how much local optical power should be used.

5.3 System Parameters and Block Diagram:

In this section a block diagram is presented and each step of the simulation is explained. This explanation also includes time- or

frequency-domain plots for some of the signals to provide visual information. The simulation uses a value of 2GHz instead of the actual THz range carrier. Also presented are the values of the parameters used and their variable names used in the program.

Modulation index[mi]=0.9

Responsivity [Resp]=1A/W

Local oscillator power[Pwr_lo] = 0.5mW

Offset frequency for the LO in (delta) = 600 MHz

Pulsewidth = 40 usec

Bandwidth = 260 MHz

Chirp rate (k) = bandwidth/pulsewidth [Hz/s]

Start frequency (w) = 2*pi*100e6 [rad/s]

Responsivity of reciver (Resp) = 1 [A/W]

Noise eqiuv power (NEP) = 2.4e-11 [A/(Hz)^.5]

Receiver BW (BW_rec) = 800e6 [Hz]

Electron Charge (q) = 1.6e-19 [Columbs]

Figure(5-6) shows the block diagram that gives a visual representation of the simulation program used and figure (5-7) shows the flow diagram of this simulation.

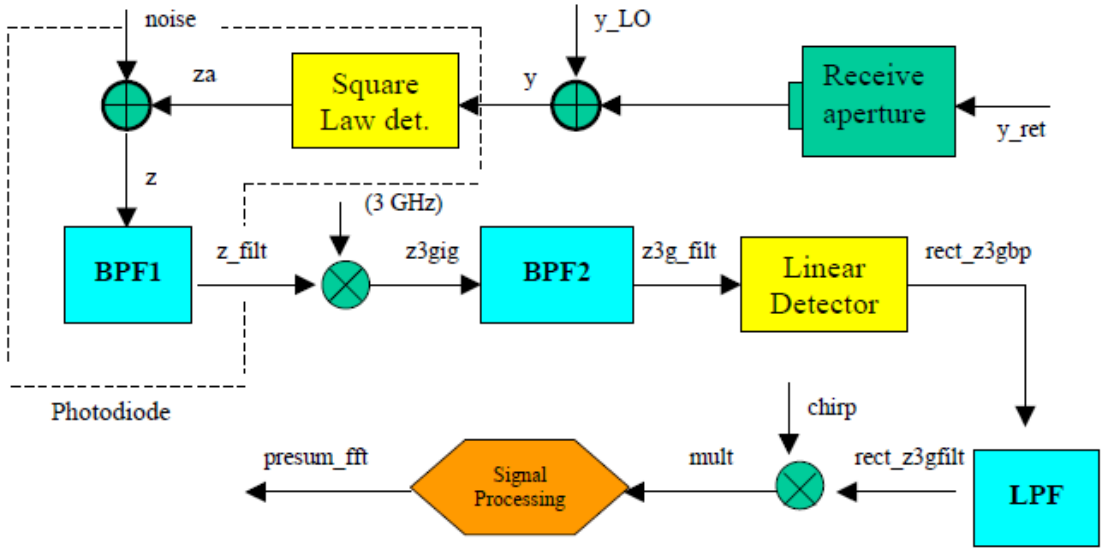

Fig. (5-6) Simulation System Diagram

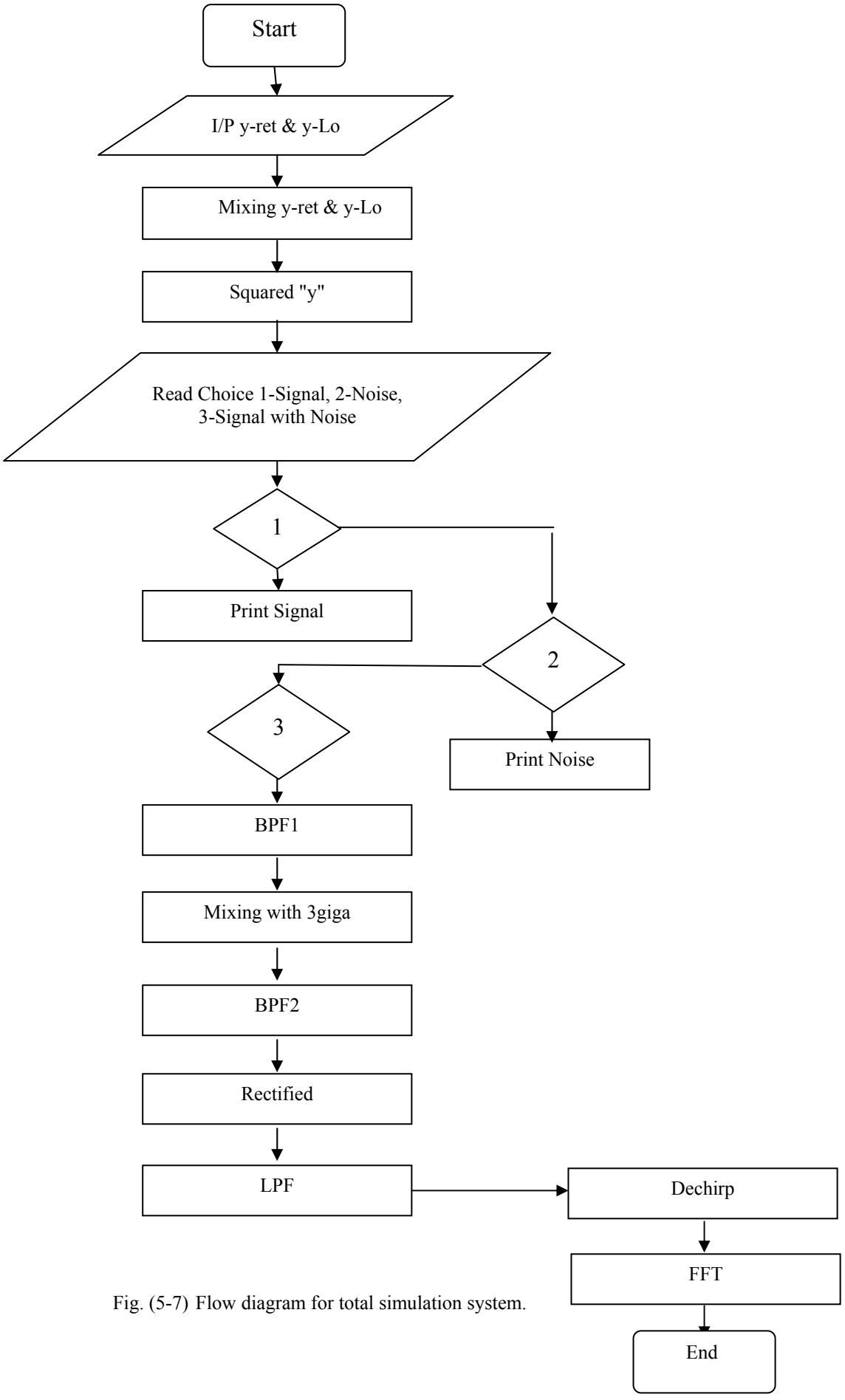

Fig. (5-7) Flow diagram for total simulation system.

As seen from figure (5-6), the simulation focuses on the receiver. This is due to the need for maximizing the receiver sensitivity for the detection of the weakest signal possible. The transmitted signal is scattered from the target and a portion reaches the receiving aperture. This signal is labeled **y_ret** can be seen in the simulation shown in figure (5-8) and is mixed with the local oscillator signal (**y_Lo**) as in figure (5-9) to simulate the coherent detection process.

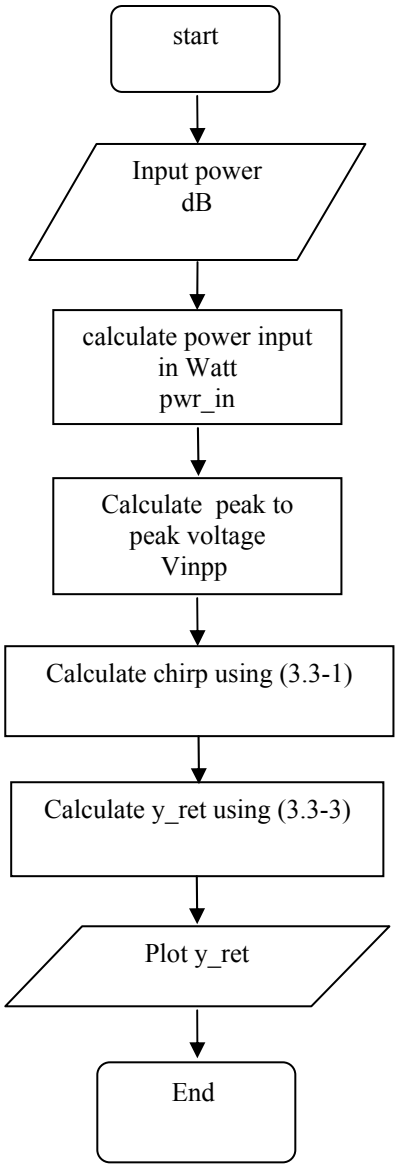

Fig. (5-8) Calculation of y_ret signal.

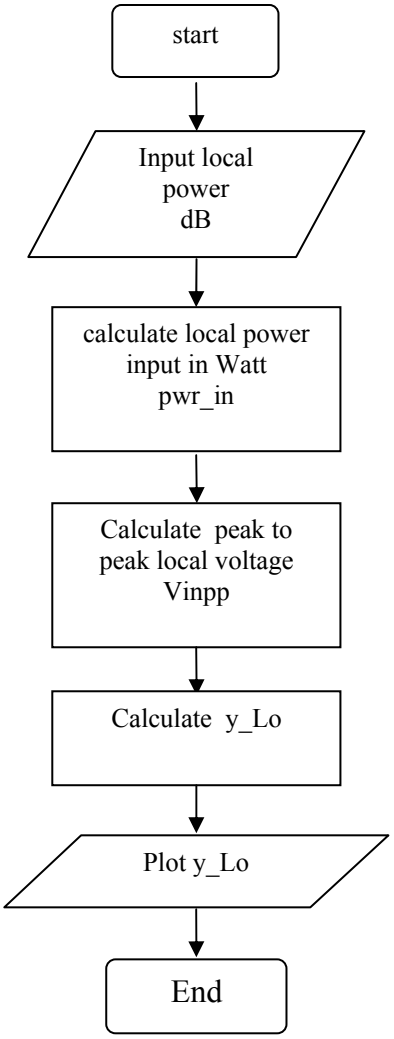

Fig. (5-9) Calculation of input local power.

The frequency-domain representations on these signals are given in figures (5-10) and (5-11), respectively. For the scattered signal, the chirp-modulated signal is seen with the carrier at 2GHz. The similar signal occurring at 8 GHz is the image signal and is not real.

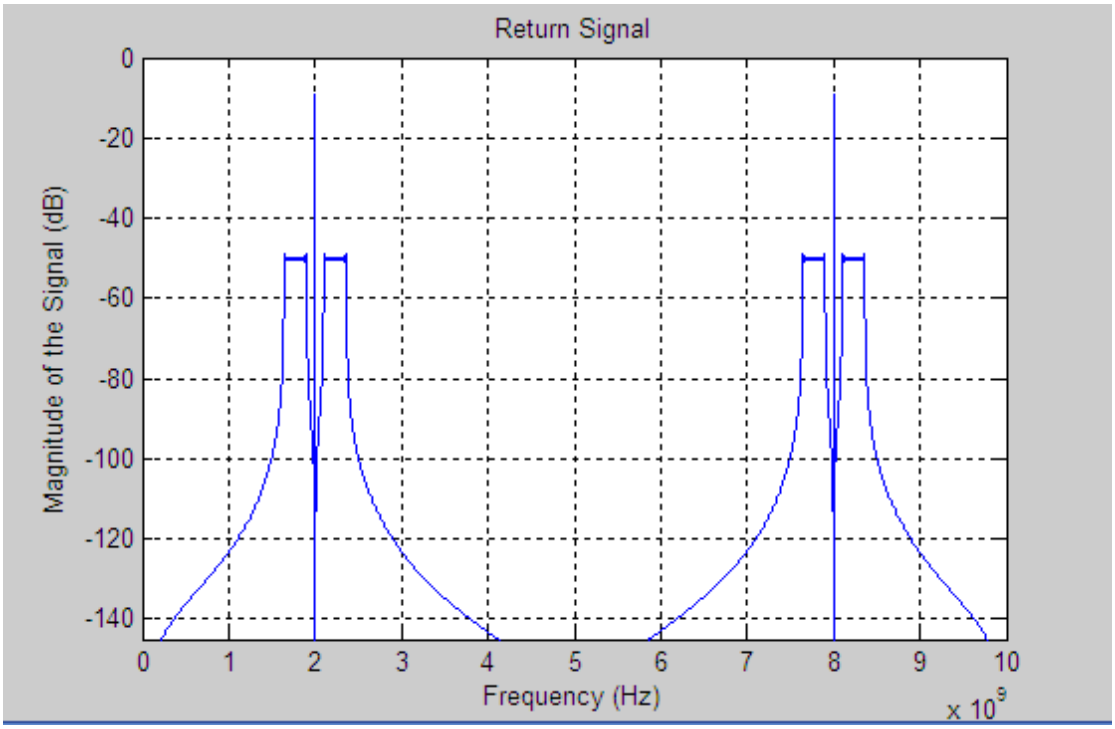

Fig. (5-10)**:** The scattered signal in frequency domain [y_ret].

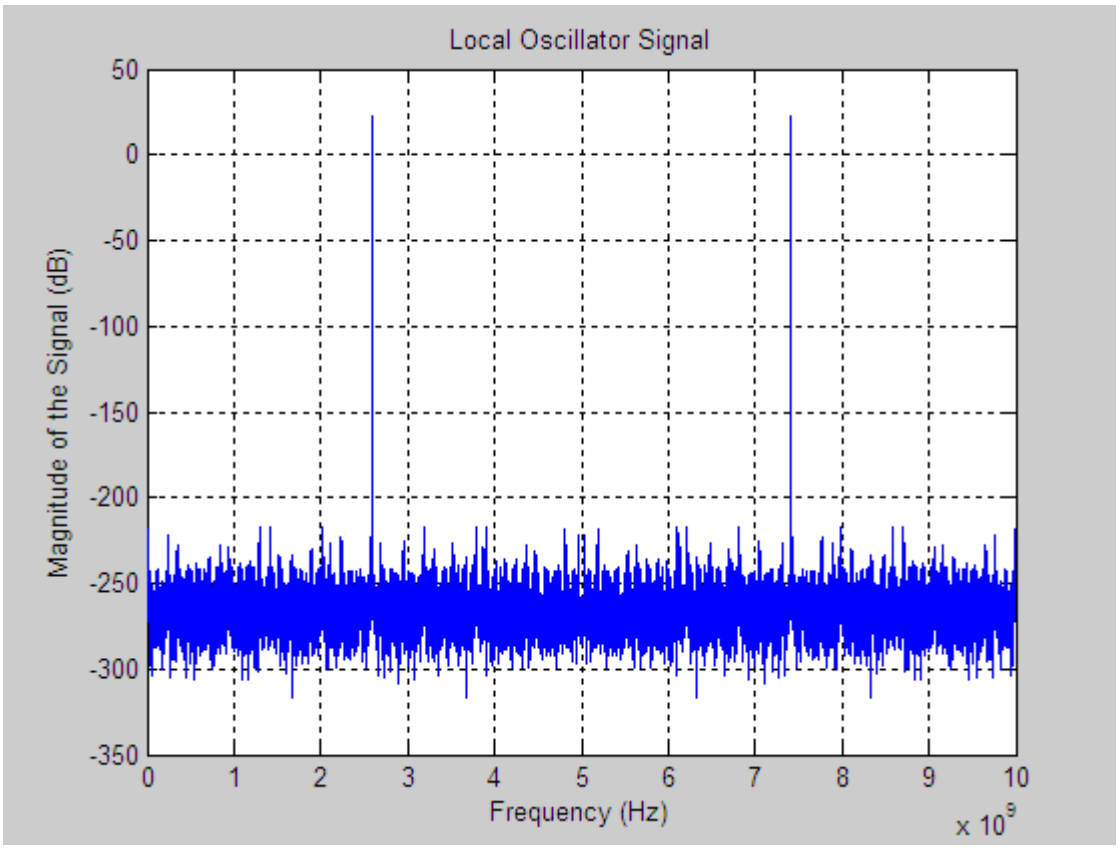

Fig. (5-11)**:** The local oscillator signal in frequency domain [y_LO].

The output of this mixer, **y**, is input to the photodiode for detection. The detection process is modeled as square-law detection as in figure(5-12), and the output of the square-law detector, **za**, is shown in figure(5-13) below.

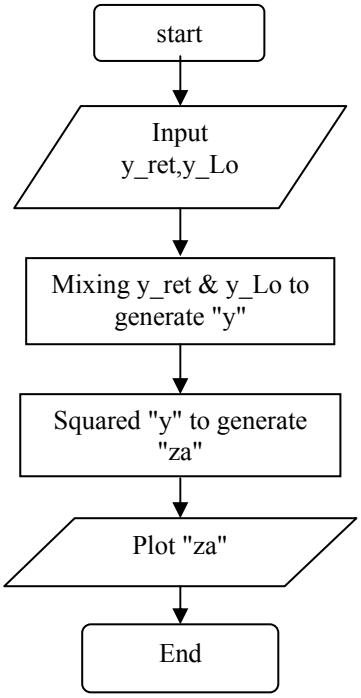

Fig. (5-12) Flow diagram to calculate "za"

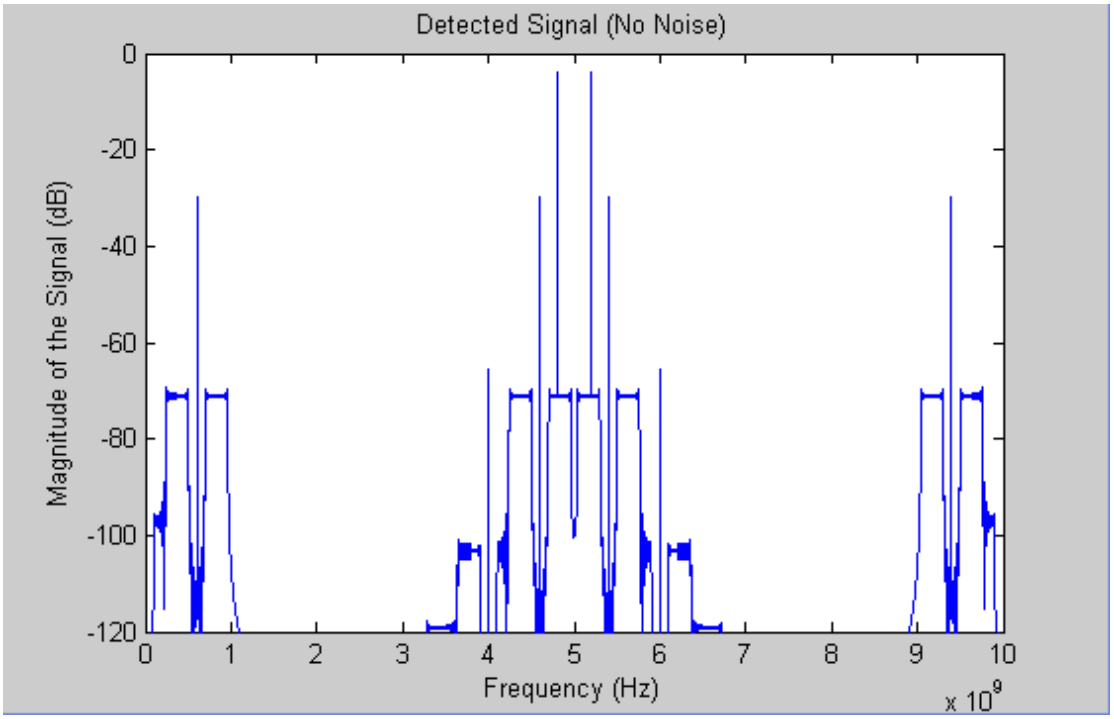

Fig. (5-13) The detected signal (no noise) in frequency domain [za].

A Gaussian noise vector, **Noise** is created and added to the detected signal to simulate the noise introduced in the photo diode. Figure(5-14) below shows the simulation operation of this process.

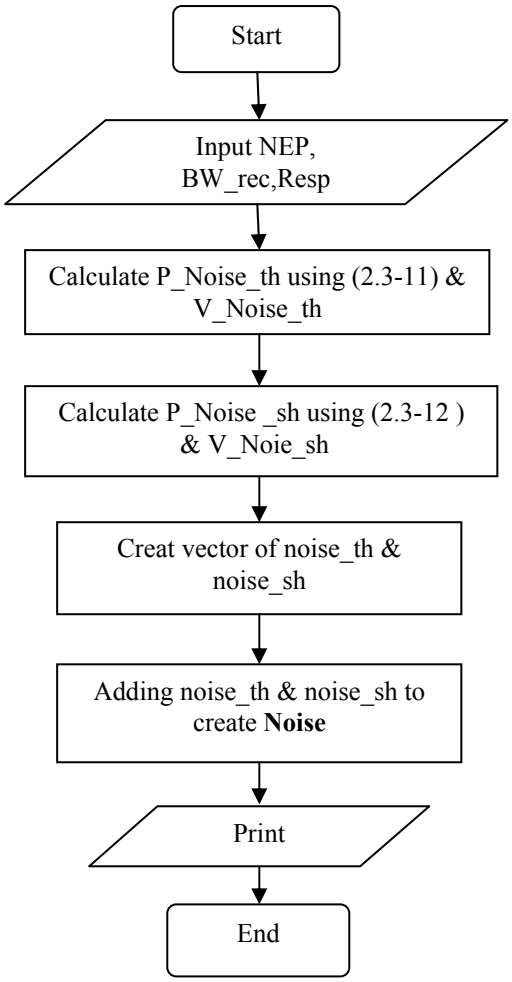

Fig. (5-14) Flow diagram for creating **Noise**

This noise vector in the simulation is obtained by creating thermal and shot noise vectors and adding them to get the **noise** vector. The detected signal with noise is, **z**, is shown in Figure(5-15) .

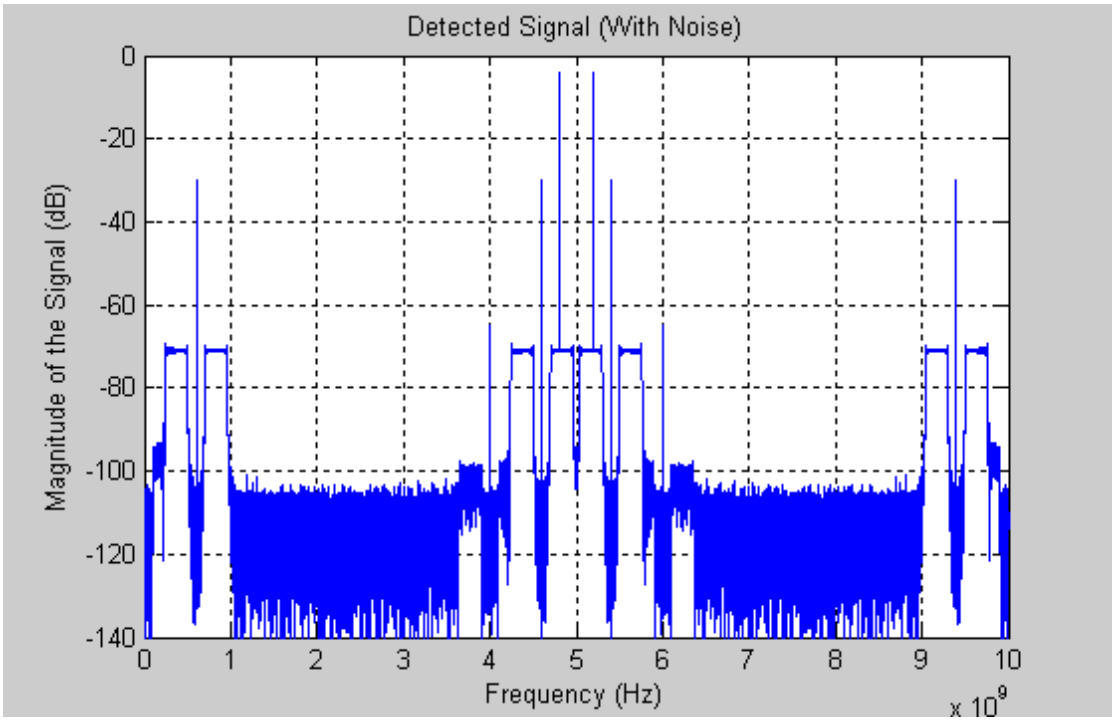

Fig. (5-15): The detected signal (with noise) in frequency domain [z].

This signal is filtered by the first bandpass filter with its lower cutoff frequency at 160 MHz and higher cutoff frequency at 1.06 GHz. This signal, **z_filt** (shown in Figure(5-16) is then multiplied by a 3 GHz signal to perform the frequency upconversion required by the linear detector.

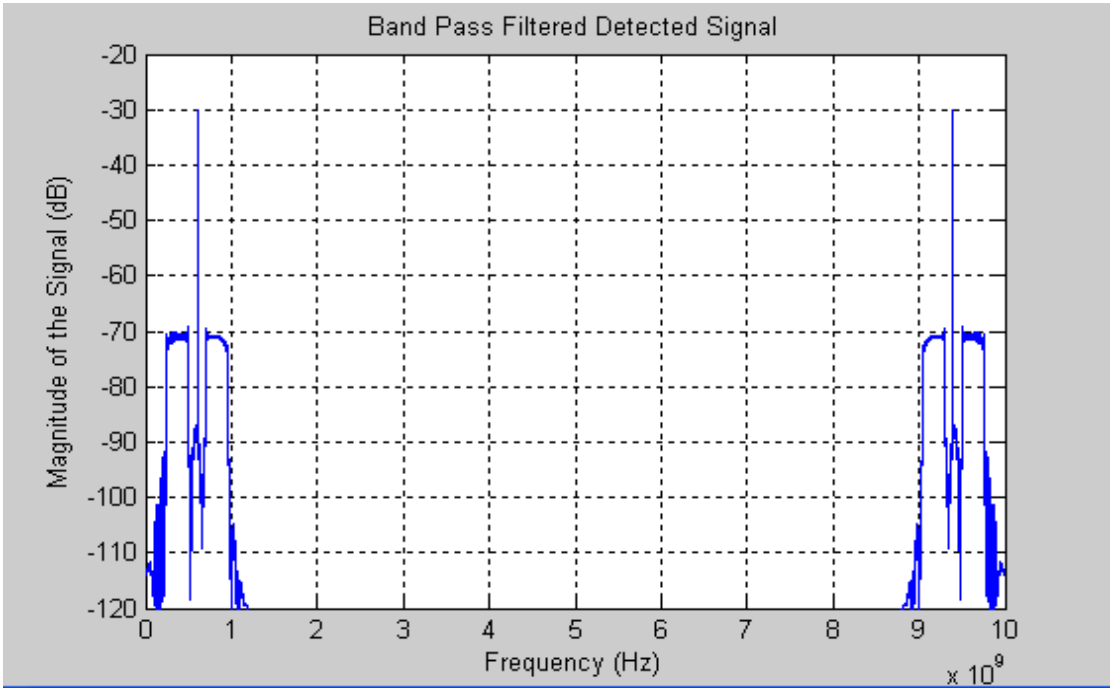

Fig. (5-16)**:** Bandpass filtered detected signal in frequency domain [z_filt].

The output of this multiplication is signal, **z3gig**, which is bandpass filtered before being sent to the envelope detector. This second bandpass filter has a passband from 3.2 GHz to 4 GHz. (The **z3gig** signal and the filtered signal **z3g_filt** are shown in Figure(5-17) and (5-18),respectively.

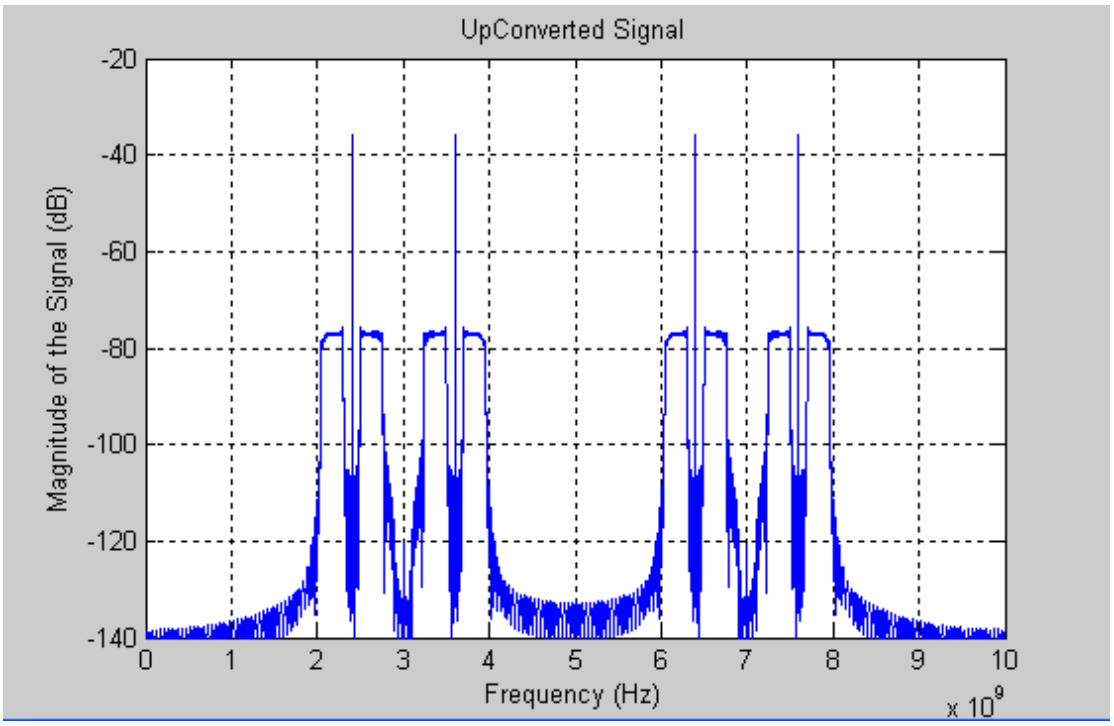

Fig. (5-17)**:** The upconverted signal in frequency domain [z3gig].

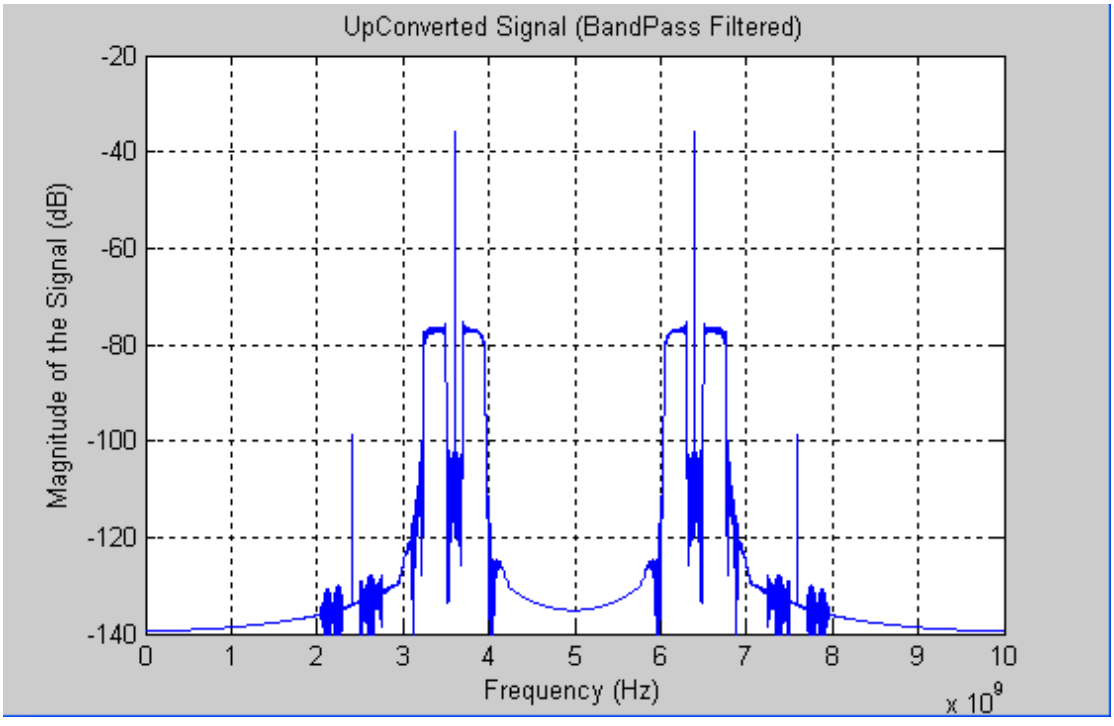

Fig. (5-18)**:** The upconverted signal (bandpass filtered) in freq. domain [z3g_filt].

The filtered signal, **z3g_filt**, is input to the module in the program that simulates linear detection (rectification) and the output signal is **rect_z3gbp**. Figure(5-19) and (5-20) show the input and output signals to the linear detector in time domain.

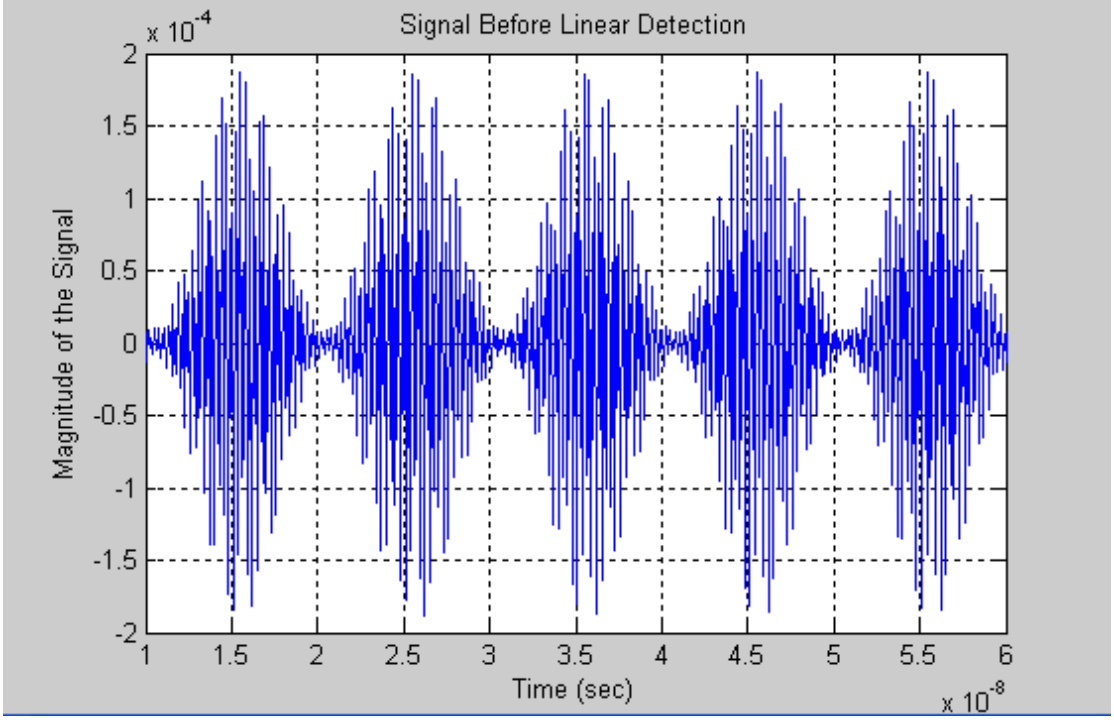

Fig. (5-19)**:** The signal input to the linear detector in time domain [z3g_filt].

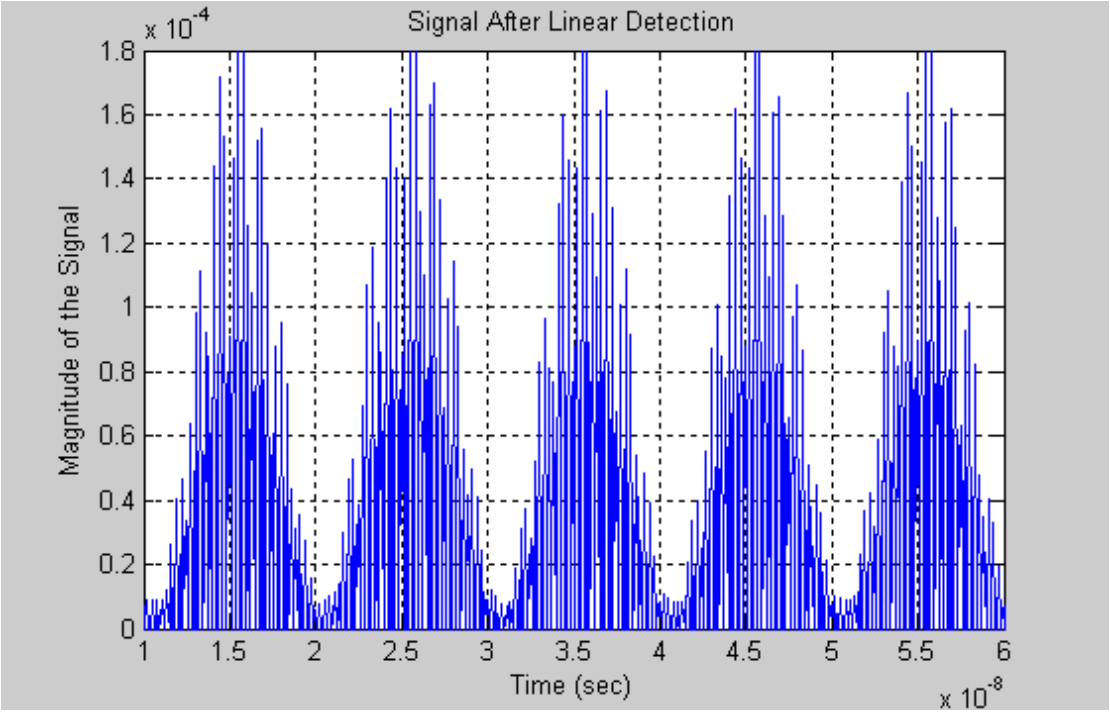

Fig. (5-20)**:** The output signal of the linear detector in time domain [rect_z3gbp].

It is then lowpass filtered and centered at zero before the dechirping process. Figure(5-21) and (5-22) show the output of this low-pass filter in both time and frequency domain.

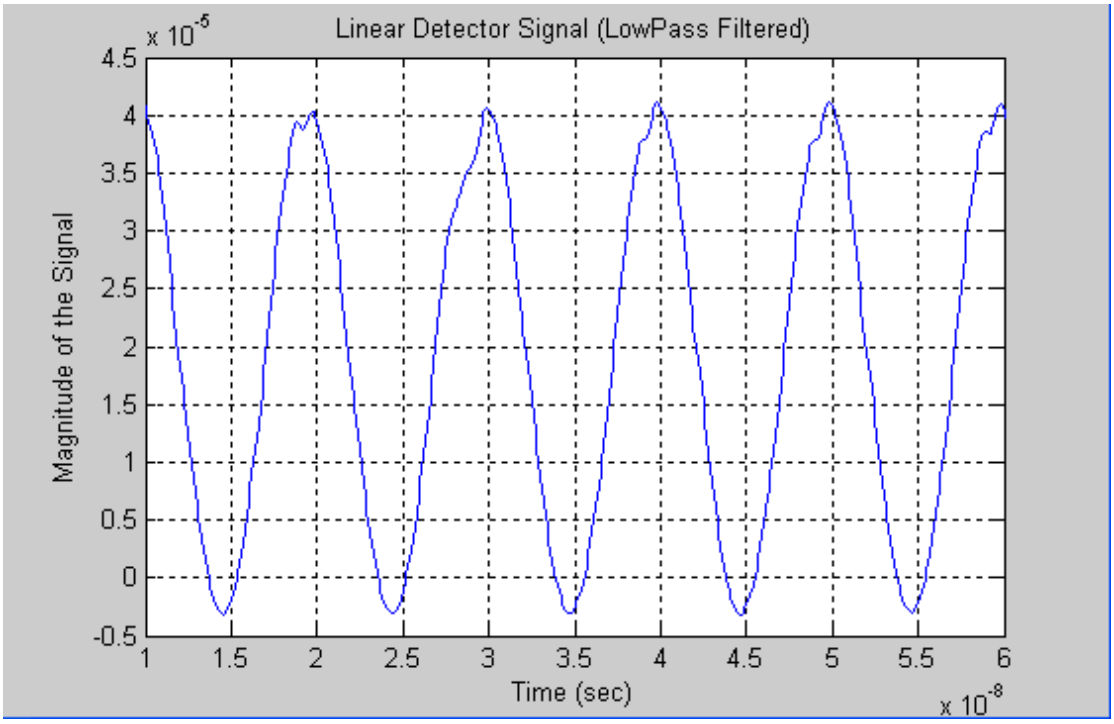

Fig. (5-21)**:** Linear detected signal (LP filtered) in time domain [rect_z3gfilt].

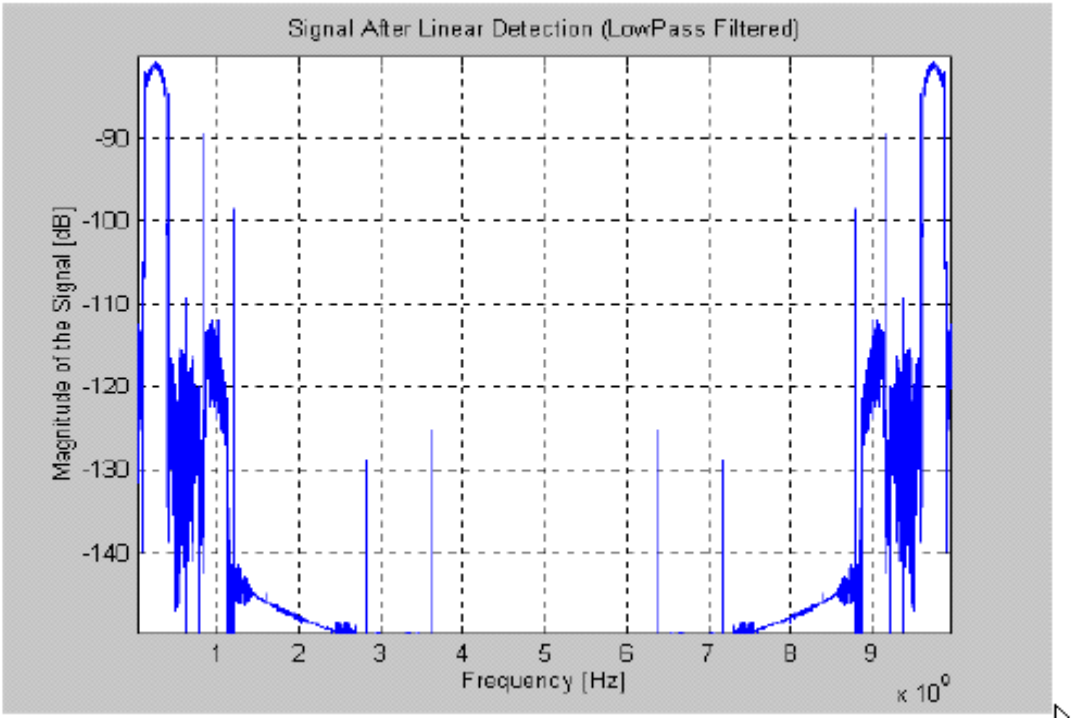

Fig. (5-22) **:** Linear detected signal (LP filtered) in freq. domain [rect_z3gfilt].

The output of the lowpass filter (**rect_z3gfilt**) is multiplied with the original chirp signal (**chirp**) to obtain the dechirped signal, **mult**. Figure(5-23) and (5-24) show this dechirped signal in time and frequency domains, respectively.

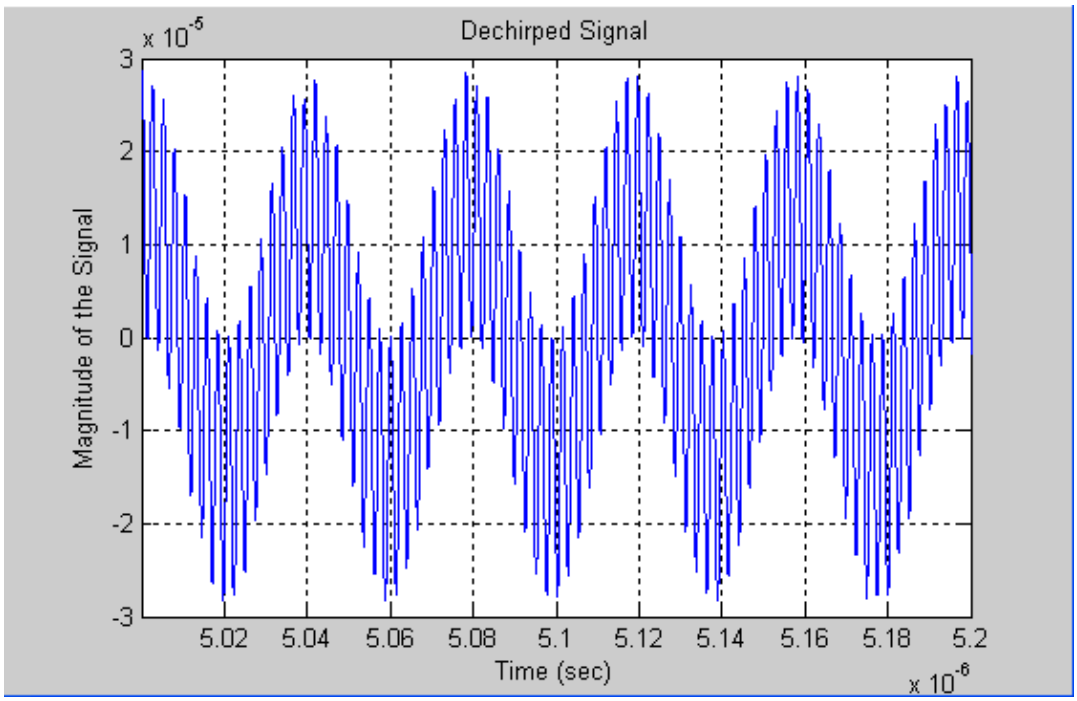

Fig. (5-23)**:** The dechirped signal in time domain [mult].

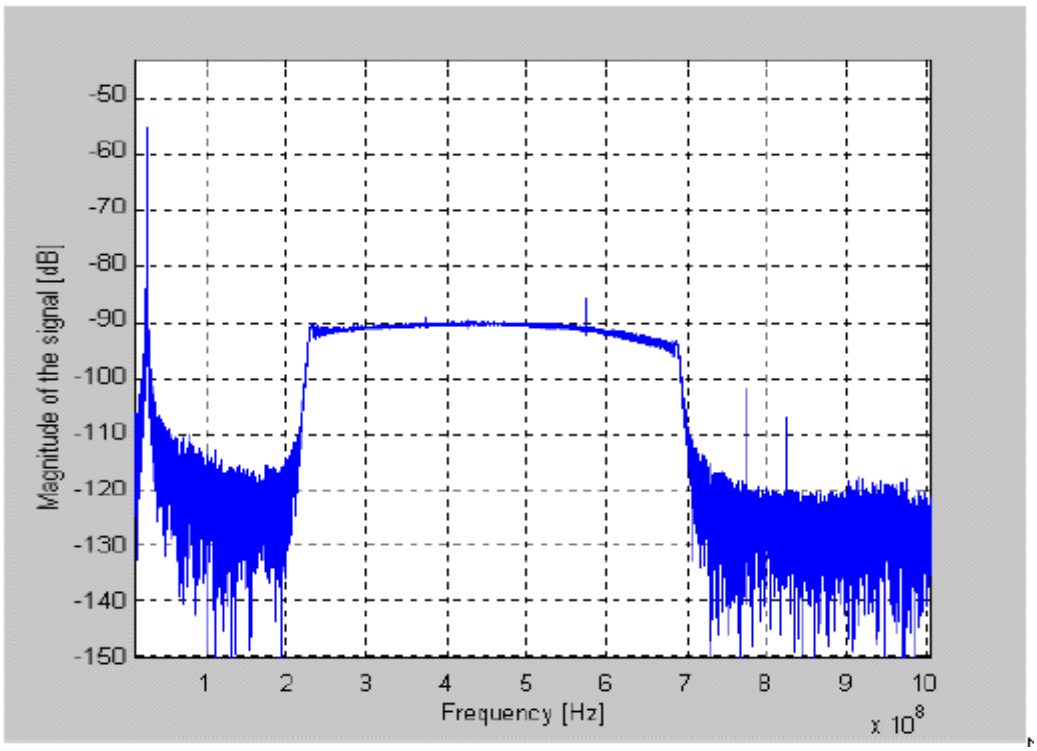

Fig. (5-24)**:** The dechirped signal in freq. domain [mult].

This signal is then sent to the signal-processing module to obtain the frequency domain representation of the **presum_fft** signal. If this signal is weak, the effects of signal processing methods like coherent integrations can be seen on this final result. Figure(5-25) shows the part of this signal spectrum that contains the frequency information for the target.

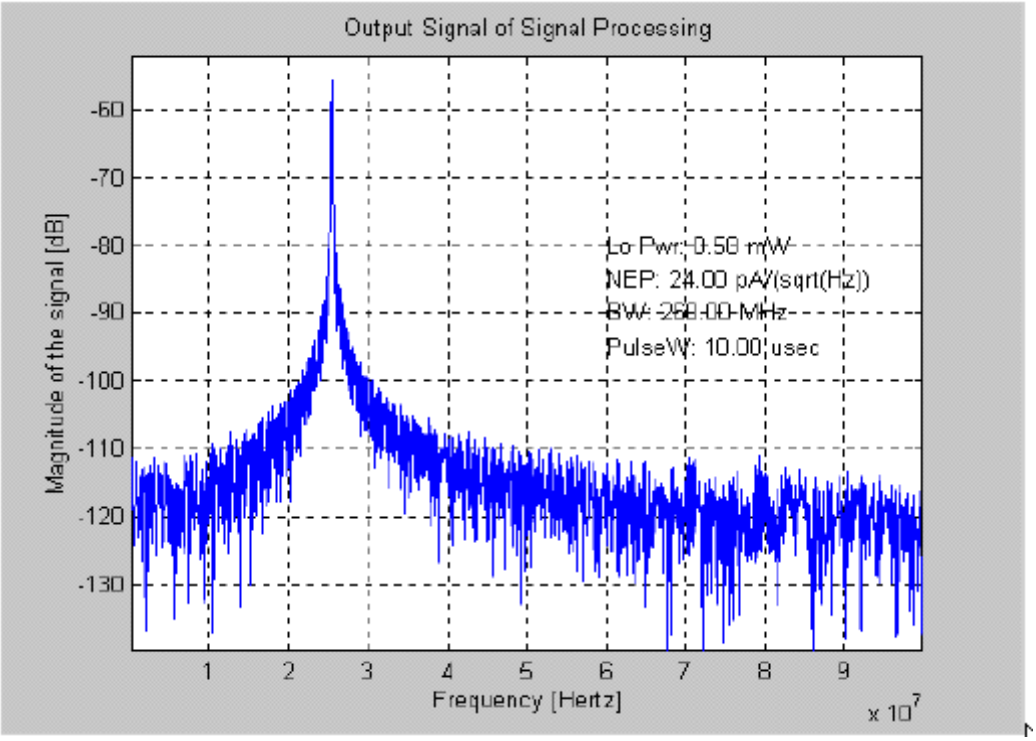

Fig. (5-25): The output of the signal processor in freq. domain [presum_fft].

5.4 The Effects of Coherent Integrations on the Output SNR of the System:

One of the important operations to be used in the system to improve system performance is coherent integration. In the most basic sense, coherent integrations average collected data to reduce the noise effects on the final result. This operation helps reduce noise since noise is random for the given segment while the signal is repetitive. The Matlab program used is modified to ask the user the number of coherent integrations performed. The number of coherent integrations is increased by an

increment of 10. Then the signal and noise powers and the signal-to-noise ratio are determined. Table(5-5) gives the results obtained from the simulation.

Table(5-5): The simulation results for testing the effects of coherent integrations on SNR.

Input Optical Powr [dBm]	**No coh int**	**Signal Power [dBm]**	**Noise Power [dBm]**	**SNR out [dBm]**
-93.01	1	-118..2	-120.35	7.6842
-93.01	10	-118.2	-130.45	12.0106
-93.01	100	-118.2	-140.15	22.4728

In this table, the first column denotes the optical power as received by the receiving aperture of the laser radar system. The second column shows how many times the received signal is averaged, while columns three to five show the signal power, noise power, and signal-to-noise ratio at the output of the receiver, respectively. These results suggest that a factor-10 increase in the number of coherent integrations increases the SNR at the output by 10 dB. This is obtained by the reduction of the noise level by 10 dB while the signal power stays the same. However, at some point the noise floor level cannot be reduced any more since the quantization noise (which cannot be reduced by coherent integration) dominates.

5.5 The Effects of Varying Modulation Index on the Minimum Detectable Optical Input Power for the System:

One of the parameters that enters into the equation for the modulated signal is the modulation index. Choosing the optimum value for the modulated signal is key since we would like to pack as much energy as possible into the transmitted pulse. As the transmitted signal's sidebands have more power, the minimum detectable signal power is lower

assuming that the attenuation through the path of the signal travels, stays constant. In order to see how changing the values for the modulation index affects the minimum detectable optical input power, P_{inopt_min} , the values for the modulation index are changed from 0.3 to 1. Then, for each case, the signal at the receiver is observed to see at which lowest input power level the output signal is still visible. This level is then labeled as the minimum detectable optical input power for that particular case. The results are presented in Table (5-6) and figure (5-26) below.

Table(5-6):Results of observing effects of changing modulation index on minimum detectable optical input power

Modulation index,u	**Minimum detectable optical input power, P_{inopt_min} [Pw]**
0.3	2.8
0.45	1.4
0.6	1
0.75	0.5
0.9	0.4
1	0.4

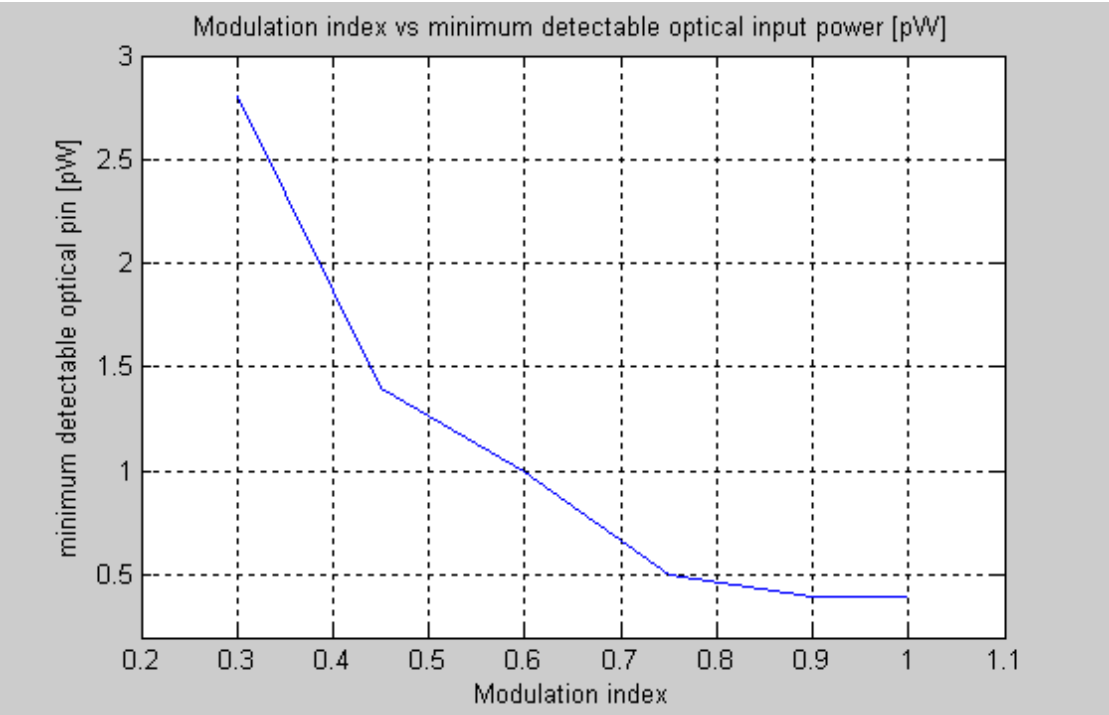

Fig. (5-26): Modulation index vs. minimum detectable optical input power.

When one observes the table (5-6) and figure (5-26), it can be noticed that as the value of the modulation index is increased from **0.3** to **1**, the minimum detectable optical input power decreases. In other words, when one uses higher values of modulation index, weaker signals can be detected which are desired. However, it is seen from the plot that this effect saturates around **0.8** and further increasing the modulation index does not improve the performance of the system. In accordance with the results of this simulation the modulation index for our system is chosen to be **1**

5.6 The Effects of Varying Noise Equivalent Power, NEP, on the Minimum Detectable Optical Input Power for the System:

Another parameter that affects the performance of the laser radar system is the photodiode's noise equivalent power, NEP. It is used to describe the noise performance of a photodetector. For a given value of thermal noise, the photodetector will have an optical power value that will cause the signal-to-noise ratio, SNR, to be equal to 1 at its output. This level of optical power is referred to as the noise equivalent power, NEP. One important point to make is that values of receiver bandwidth and operating temperature should be specified to make the value of the NEP meaningful for each detector. To see how changing the values for the NEP affects the minimum detectable optical input power, P_{inopt_min} ,it is modified and the values for the NEP are changed from **2.4** pA / Hz to **240** pA / Hz . Then, for each case, the signal at the receiver output is observed in order to see at which lowest input power level the output signal is still detectable. This level is then labeled as the minimum detectable optical input power for that particular case. The results are presented in table(5-7) and figure(5-27).

Table (5-7): The effects of NEP on minimum detectable optical input power.

NEP [pA/sqrt[Hz]	Minimum detectable optical input power, Pinput_min[pW]
2.4	0.0047
12	0.1
24	0.38
120	11.2
240	28

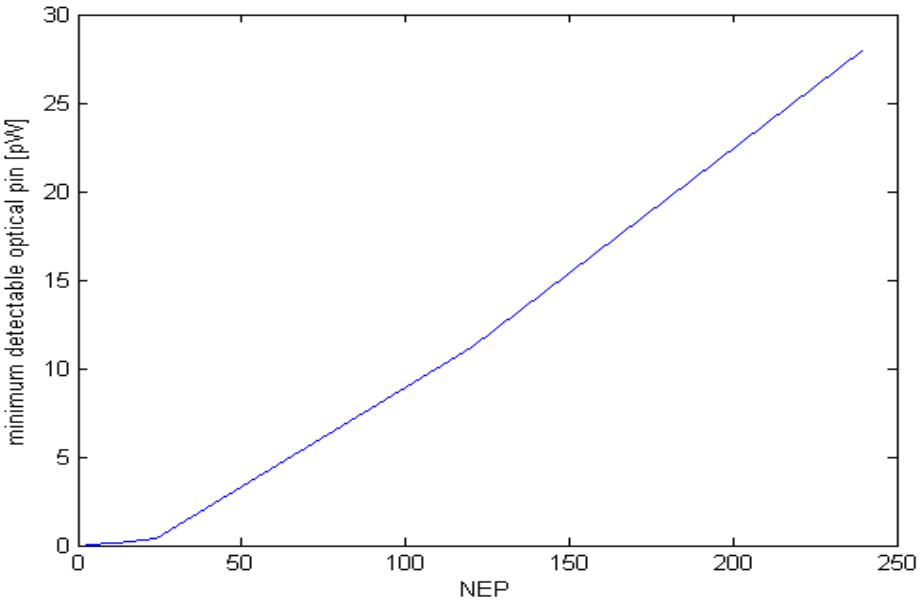

Fig. **(5-27):** NEP vs. minimum detectable optical input power.

When the results are observed, one can notice that when the NEP is smaller, the system can detect weaker signals. This is expected since a smaller NEP means less noise in the photodetector giving way to weaker signals to be detected. In the end, the photodetector with the smallest NEP is chosen for the laser radar system.

5.7 The Effects of Varying Local Oscillator Power, P lo, on the Minimum Detectable Optical Input Power for the System:

The local oscillator power plays an important role in determining the minimum detectable optical input power for the system. This is because it mixes with the incoming optical signal before the square-law detection process. At the output of the detector the signal to be further analyzed is the cross term that is affected by the incoming signal power and the local oscillator power. A better way to see this term is to look at the mathematical model for the square-law detection:

$$(P_{input\_opt} + \mathrm{P\_Lo})^2 = P_{input\_opt}{}^2 + P\_Lo^2 + \mathbf{2(P_{input\_opt}\, P\_Lo)} \qquad (5\text{-}1)$$

Where

P_{input_opt} = input optical power

P_Lo = local oscillator power

The term in bold in equation (5-1) is the cross term of the input signal power and the local oscillator power, and it is the term analyzed in the receiver to get target information needed. This term clearly shows that the local oscillator power plays an important role in obtaining target information. To see how changing the values for the local oscillator power affects the minimum detectable optical input power, the values for the local oscillator power are changed from 0.05 mW to 5 mW. Then, for each case, the signal at the receiver output is observed to see at which lowest input power level the output signal is still visible. This level is then chosen as the minimum detectable optical input power for that particular case. The results are presented in Table 5-8 and Figure(5-28).

Table 5-28: The effect of changing the local oscillator power on minimum detectable input power.

Local Oscillator Power (P_Lo) [mW]	**Minimum detectable optical input power, Pinput_min[pW]**
0.05	3.6
0.50	0.36
5.00	0.036

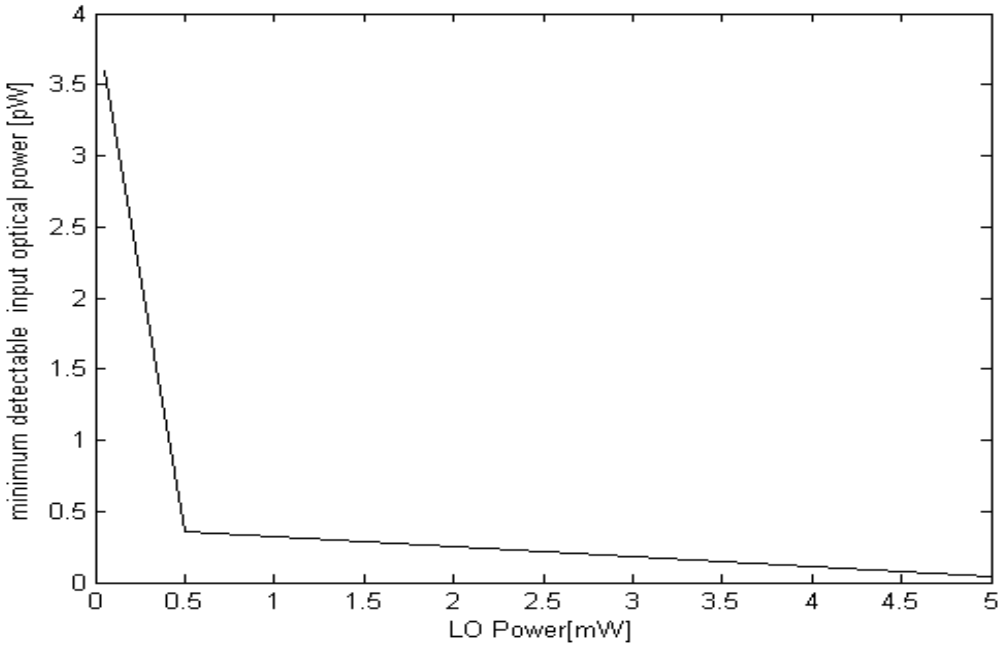

Fig. **(5-28)**: LO power versus minimum detectable input optical power.

As can be seen from the results presented, the lower the value for the local oscillator power, the stronger the incoming signal needs to be detected. In other words, to be able to detect weaker signals, the local oscillator power needs to be kept at its highest value.

Chapter Six

Conclusions and Future Recommendations

6.1 Conclusions:

In view of the results presented in this study, the main contributions of this research can be summarized as follows:

1- From study and analyze when the incoherent detection scheme was used, the SNR obtained was –132 dB, which is too low for accurate range measurement**.**

2- To improve this SNR, we used coherent detection, which provided an improvement of 94 dB with a Plo of 1 mW.

3- To further improve the SNR of the system, the pulse compression technique is introduced. With this technique, a chirp rate of k = 260 MHz/ 40 μs provided a 40 dB SNR improvement.

4- The system's data collection is configured to perform 10 coherent integrations, which brought the system's SNR to about 12dB.

5- With all these techniques, one can measure the range to a target at 600km with a range accuracy of 10cm with a peak transmit power of 10mW.

6- One of the simulations predicted is the effect of value of modulation index on the mimimum detectable optical input power; its optimum value is predicted with the simulation results. The results show that the higher its value is to the maximum (which is 1), the better. This is determined by finding the minimum detectable optical input power possible for different values of modulation index.

7- The NEP's effect on the minimum detectable optical input power is observed. When the value of NEP is varied, we see that when the NEP is smaller, the system can detect weaker signals.

8- The optimum value for the local-oscillator signal power is predicted by observing the effects of its change on the minimum detectable input power. As expected, the higher the value for the

LO power, the better weak signals are detected. Hence, the LO power value is to be chosen as high as possible within the system's capabilities.

6.2 Future Work:

- Other technique such that homodyne detection and I and Q detection schemes, can be investigated.
- The mathematical modeling and simulation of the system is recommended to be constructed and tested experimently to verify the system performance
- Other areas of future work could investigate the benefits of excess pulse width, operation in FM-CW mode and the use of large-core multimode fiber instead of single-mode fiber.
- A scanner configuration, where the transmitted signal scans an area rather than a point, is suggested.

References:

1- Jelalian, "Laser Radar Systems", Artech House, Norwood, MA., (1992).

2- I. Renborn, O. Steinvall and A. Widen, "Performance Study of a Coherent Laser Radar", *Proc. SPIE* Vol.415, pp.39-50 (1983).

3- Thomas J. Kane, W.J.Kozlovsky and Robert L.Byer, "Coherent Laser Radar at 1.06um Using Nd:YAG Lasers", *Opt. Lett.*, vol.12(4),pp.239-241(1987).

4- Jeffrey K. Bounds, "The Infrared Airborne Radar Sensor Suite", Institute of Technology Cambridge, RLE Technical Report No. 610, (1996).

5- Eric Blanquer, "LADAR Proximity Fuze - System Study", Thesis, Sweden, Stockholm, *XR-EE-RT* 2007:009, (2007).

6- M. Harris, "Lidar for Turbine Control", National Renewable Energy Laboratory Golden, Colorado, Technical Report NREL/TP-500-39154,(2006)

7- Slava G. Turyshev, "Detection of Optical Radiation", EE692 Presentation, (2006).

8- Robin R. Burton, et al, "Elastic LADAR Modeling for Synthetic Imaging Applications", Thesis, Rochester Institute of Technology, (2006).

9- E.D. Hinkley, ed, "Laser Monitoring of the Atmosphere, *Springer*, *Berlin* (1976).

10- Takashi T., "Nobuhiro Saga and Otozo Fukumitsu, Optical of an Airy Signal Field with a Gaussian Local-Oscillator Heterodyne Field", *Electronic and Communications in Japan*, vol. 63-c (7), pp. 101-107 (1980).

11- K.Hulme, B. S. Collins, G. D. Constant, J. T. Pinson, "A CO_2 Laser rangefinder Using Hetrodyne Detection and Chirp Pulse

Compression", *Optical and Quantum Electronics*, Vol. 13, 35-45 (1981)British Crown.

12- I. Rethorn, O. Steinvall, D. Letalick, K. Gulberg, "Performance Study of a Coherent Laser Radar", *Proc. SPIE* vol. 415, pp. 39-50 (1983).

13- J. Satzman and A. Katzir, "Hetrodyne Detection SNR: Calculations with matrix Formalism", *Appl. Opt*., Vol. 23(7), pp.1066-1074(1984).

14- J. Bilbro, G. Fichtl, D. Fitzjarrald, and M. Krause, "Airborne Doppler Lidar Wind Field Measurements", *American Meteorological Society*, vol. 65(4), pp. 348-359 (1984).

15- Bilbro, J.W., C. DiMarzio, D. Fitzjarrald, S. Johnson and W.D. , "Airborne Doppler lidar measurements", *Appl. Opt.* 25(21), 3952-3960, (1986).

16- Thomas J. Kane, W. J. Kozlovsky, and Robert I. Byer, "Coherent Laser Radar at 1.06 um Using Nd:YAG Lasers", *Opt. Lett*., vol. 12 (4), pp. 239 -241 (1987).

17- Walter L. Tucker and John L. Barret, "Hetrodyne Efficiency of Quadrant Photodetectors", *Appl. Opt.* 28(5), 892-896 (1989).

18- Rao, M. K. and Goh, C. C. "A Low-cost near-IR Laser Radar" *IEEE photonics Technology Letters*, vol. 2, P.(683-5), (1990).

19- Ullrich and Andreas Gerhard, "High resolution Optical Doppler Radar" Technische universtaet Wine(Austria), (1990).

20- Pleshanov YU. and Fratini TA., "Coherent Reception of An Optical Signal in Laser Surveillance Radar Systems", *Soviet Journal of Optical Technology*. (1993).

21- Irene Fung, "Multiresolution Laser Radar Range Profiling with the Expection-Maximization Algorithm", Utah State University, (1994).

22- Kawakami T., "Adaptive Multifrequency Modulation Method for an Advanced Laser Range Finder", *IEEE Transactions on*

Instrumentation and Measurement, P. (857-860), (1995).

23- Der S. and Redman B. "Simulation of Error in Optical Radar Range Measurements". *Appl. Opt.*, P.(6869-6874), (1997).

24- Ikuta. K. Kudo T. and Vasa NJ. "Geometrical form Factor Improvement for Receiving System of Infrared Lidar", *Optical Review*, p.(464-470),(1999).

25- J. Bryan Blair, David L. Rabine, and Michelle A. Hofton, "The Laser Vegetation Imaging Sensor: a medium-altitude", *ISPRS Journal of Photogrammetry & Remote Sensing* 54 115– 122(1999).

26- Steinvall O. , "Effects of Target Shape and Reflection on Laser Radar Cross Sections Source", *Appl. Opt*., P4381- 4391,(2000).

27- Avril Behan, "On the Matching Accuracy of Rasterised Scanning Laser Altimeter Data", *IAPRS*, Vol. XXXIII, Amsterdam, (2000).

28- Andreas Olsson, "Target recognition by vibrometry with a coherent laser radar", LiTH-ISY-EX-3050-2003 Linköping (2003).

29- Robert L. Lucke, "Synthetic Aperture Ladar Simulations with Phase Screens and Fourier Propagation",*IEEE* 0-7803-81 55-6/0461, 2004).

30- Lars Sjöqvist‡, "Markus Henriksson and Ove Steinvall, "Simulation of laser beam propagation over land and sea using phase screens a comparison with experimental data", *Proc. of SPIE* vol. 5989,9890D, (2005) .

31- Vesna Ducic1, Markus Hollaus1, Andreas Ullrich2, Wolfgang Wagner1 and Thomas Melzer1, "3D Vegetation Mapping and Classification Using Full-Waveform Laser Scanning", Workshop on 3D Remote Sensing in Forestry, (2006).

32- Benjamin Koetz, Guoqing Sun, Felix Morsdorf and K.J. Ranson , "Fusion of imaging spectrometer and LIDAR data over combined radiative transfer models for forest canopy Characterization", *ScienceDirect* RSE-06685, (2006).

33- Wallace, Sung and Buller, Detecting and Characterising returns in a pulsed ladar System, *IEEE* Proc. vol. 153,No.2 (2006).

34- Qunig-wei and Gui-fen, "Study on the Weak Signal Detection in the Laser Radar Based on the Chaos Theory", *Proc. of SPIE* Vol.6622, 66220O, (2008).

35- M. I. Skolnik, ed., *"Radar Handbook", New York: Artech House*, (1970).

36- M. I. Skolnik, "Introduction to Radar Systems", *New York: Artech House*, 2nd ed., (1980).

37- E. Brookner, ed., "Aspects of Modern Radar" Boston: *Artech House*, 1988.

38- J. W. Goodman, "Introduction to Fourier Optics" McGraw-Hill Physical and Quantum Electronics Series, *New York: McGraw-Hill Book Company*, (1968).

39- J. H. Shapiro, B. A. Capron, and R. C. Harney, "Imaging and target detection with a heterodyne-reception optical radar", *Appl. Opt*. 20, 3292-3313 (1981).

40- Papurt, D.M., Shapiro, J.H., and Harney, R.C., "Atmospheric Propagavion. Effects on Coherent Laser Radars," *Proc. SPIE* 300, 86-99 (1981)

41- Harrison, NJ, "RCA Electro-Optics Handbook" : *RCA Corporation, RCA Commercial Engineering*, 2d ed., (1974).

42- N.E. Zirkind and J.H. Shapiro, "Adaptive Optics for Large Aperture Coherent. Laser Radars", *Proc. SPIE* 999, 117 (1988).

43- J. H. Shapiro, "Imaging and optical communication through atmospheric turbulence, in Laser Beam Propagation in the Atmosphere" *Appl. Phys*., chapter 6, 171-222, (1978).

44- Shapiro, J.H., "Target-Reflectivity Theory for Coherent Laser Radars", *Appl. Opt.* 21, 3398-3407 (1982).

45- R. H. Kingston, " Detection of Optical and Infrared Radiation", Berlin: Springer-Verlag, (1978).

46- J.H. Shapiro, R.W. Reinhold, and D. Park, "Performance analyses for peak- detecting laser radars," *Proc. SPIE* 663, 38-56 (1986).

47- S. M. Sze, "Physics of Semiconductor Devices" *New York: John Wiley & Sons*, (1981).

48- R. H. Kingston, "Detection of Optical and Infrared Radiation", Berlin: Springer-Verlag, (1978).

49- S. M. Sze, "Physics of Semiconductor Devices" *New York: John Wiley & Sons*, (1981).

50- A. Yariv, "Optical Electronics" *Holt, Reinhart and Winston*, 3rd ed., (1985).

51- Christopher Allen, Yanki Cobanoglu and Sekken Kenny, "Development of a 1319 nm Laser Radar using Fiber-Optics and RF Pulse Compression: Receiver Characterization", *Radar Systems and Remote Sensing Laboratory*, Kansas 66045-7609 (2003).

52- Yanki Cobanoglu, Sekken Kenny Chong, and Sivaprasad Gogineni, " Performance of a 1319 nm laser radar using RF pulse compression", Radar Systems and Remote Sensing Laboratory *USA,* 66045-7612 (2001).

53- Christopher Allen, Sekken Kenny Chong, and Yanki Cobanoglu," Test results from a 1319-nm laser radar with RF pulse compression", Radar Systems and Remote Sensing Laboratory *USA,* 66045-7613 (2002).

54- Bassem R. Mahafza, "Radar Systems Analysis and Design Using MATLAB" by CHAPMAN and HALL/CRC (2000).

55- Lillesand, M., and R. W. Kiefer, "Remote Sensing and Image Representation", *John Wiley & Sons, Inc, New York City*, (1987).

56- Green, P. E., "Fiber Optic Networks", *Prentice-Hall, New Jersey*, (1993).

57- Liu, M., "Principles and applications of optical communications", Irwin Book Team, Chicago, (1996).

58- Bassem R. Mahafza, "MATLAB Simulation for Radar Systems Design" CHAPMAN and HALL/CRC (2004).

59- Michael O. Kolawole, "Radar Systems, Peak Detection and Tracking" ,Mchael Kolawole , (2002).

60- Allen, C., "Analysis of a Digital Chirp Synthesis", Exploratory Radar Development, Sandia National Laboratories, Albuquerque, New Mexico, August, (1988).

61- Peebles, P. Z., Jr., "Radar Principles", *John Wiley & Sons, New York City*,(1998).

62- Stimson, G. W., "Introduction to Airborne Radar", 2nd ed., *Scitech Publishing, New Jersy*, (1998).

جمهورية العراق
وزارة التعليم العالي والبحث العلمي
الجامعة التكنولوجية
قسم هندسة الليزر والبصريات الألكترونية

محاكاة حاسوبي لأداء الرادار الليزري

اطروحة

مقدمة الى قسم هندسة الليزر والبصريات الألكترونية –الجامعة التكنولوجية وهي جزء من
متطلبات نيل درجة الدكتوراة في فلسفة هندسة الليزر والبصريات الألكترونية

من قبل

حميد فياض عفج الخزرجي

(بكالوريوس هندسة كهربائية 1979)

(ماجستير بصريات الكترونية 2001)

اشراف

أ.م.د- حسين جمعة عباس

1429هـ 2009م

الخلاصة

تلعب أ نظمة الرادار الليزرى دورا مهما فى تطبيقات مراقبة التغيرات المناخية الشاملة لامتلاكها دقة فى التحليل المكانى والمديات. ان انظمة الرادار الليزرى المبنية حاليا تستخدم نبضات ذات عرض قليل وطاقة عالية مما يجعل استخدامها على نحو نموذجى وبتكرارية معتدلة لغرض اطالة عمراللیزر المستخدم فى هذه التطبيقات. ان فكرة استخدام مصدر ليزري مستمر بطول موجي مقداره 1319 نانومتر وقدرة قصوى مقدارها 20 ملي ديسبل وبعرص نطاق 5 كيلوهيرتز ومحملة بأشارة السقسقة عرضها 40مايكروثانية وعرض حزمة 260ميكاهرتز لغرض االحصول على نسبة خطأ في المدى 10سم وبدقة تحليل مقدارها 0،576 م التي تتوافق مع انظمة الرادار الليزرى التى تسخدم نبضات قصيرة وطاقة عالية قد تم ايضاحها. من خلال التحليل والحسابات اثبتت النتائج ان استخدام الكشف البصري المتشاكه والنبضات الراديوية المضغوطه وعملية توحيد التشاكه (دمج اشارات مختلفة ومعالجتها رياضيا للحصول على حالة واحدة) يحسن في الربحية للأشارة بمقدار 94 ديسيبل , 40 ديسيبل و10 ديسيبل على التوالي. وهذه العملية حققت أعلى حساسية للمستلمة والتي تكون متوافقة مع القدرات الواطئة لليزر. بعد تحديد متغيرات الرادار الليزري واكمال النموذج الرياضي أصبحت عملية المحاكات باستخدام برنامج الماتلاب سهلة للتنبأ في سلوك الرادار الليزري تحت ظروف ومتغيرات مختلفة. أوضحت نتائج المحاكات تأثيرا لمتغيرات التالية : معامل التضمين والقدرة المكافئة للضوضاء والقيمة المثلى لقدرة المذبذب المرجعي لكشف اقل قدرة داخلة للكاشف. بينت النتائج ان اعلى قيمة لمعامل التضمين والتي قيمتها مساوية الى واحد هي ألأفضل وان نظام المستقبلة يكشف ألأشارة الضعيفة عندما تكون القدرة المكافئة للضوضاء صغيرة وان قيمة قدرة المذبذب المرجعي يتم اختيارها كأعلى قيمة قدر ألأمكان لغرض كشف ألأشارات الضعيفة.